Improved Automated Diagnosis of Misfire in Internal Combustion Engines Based on Simulation Models

Jian Chen[1, 2*], Robert Bond Randall[1]

1. School of Mechanical and Manufacturing Engineering, University of New South Wales, Sydney 2052 Australia
2. Institute of Sound and Vibration Research, University of Southampton, Southampton SO17 1BJ, UK

Telephone: +44-758-7456129
Email: jian.chen1@unsw.edu.au; jc2d14@soton.ac.uk

Abstract

In this paper, a new advance in the application of Artificial Neural Networks (ANNs) to the automated diagnosis of misfires in Internal Combustion engines(IC engines) is detailed. The automated diagnostic system comprises three stages: fault detection, fault localization and fault severity identification. Particularly, in the severity identification stage, separate Multi-Layer Perceptron networks (MLPs) with saturating linear transfer functions were designed for individual speed conditions, so they could achieve finer classification. In order to obtain sufficient data for the network training, numerical simulation was used to simulate different ranges of misfires in the engine. The simulation models need to be updated and evaluated using experimental data, so a series of experiments were first carried out on the engine test rig to capture the vibration signals for both normal condition and with a range of misfires. Two methods were used for the misfire diagnosis: one is based on the torsional vibration signals of the crankshaft and the other on the angular acceleration signals (rotational motion) of the engine block. Following the signal processing of the experimental and simulation signals, the best features were selected as the inputs to ANN networks. The ANN systems were trained using only the simulated data and tested using real experimental cases, indicating that the simulation model can be used for a wider range of faults for which it can still be considered valid. The final results have shown that the diagnostic system based on simulation can efficiently diagnose misfire, including location and severity.

Keywords: misfire diagnosis, Internal Combustion engines, Artificial Neural Networks, simulation, torsional vibration

1. Introduction

Misfire is a very common combustion fault for IC engines and many works have been put forward to study vibration-signal-based misfire diagnosis. The vibration based misfire diagnosis can be further divided into two types: one is based on the translational acceleration signals measured on the engine block, while the other is based on the torsional vibration signal of the crankshaft. The acceleration signals contain more information about high frequency components while the torsional vibration can give more precise information about low frequency components. Some research [1-7] has looked at using translational acceleration signal measurement for the misfire diagnosis. This approach involves recording vibrations at a position either on the engine block or on the cylinder head and requires the design of an appropriate inverse filter, usually in the form of a parametric model. In contrast, more research [8-19] has been done on misfire diagnosis based on the crankshaft angular vibration signal. For small engines with nearly rigid crankshafts, it can be considered that there is a linear relationship between the chamber pressure and torsional vibration, and using torsional vibration for the misfire diagnosis should be reliable under this condition. But for the bigger engines with long and flexible crankshafts, the combustion in different cylinders has a different effect on torsional vibration response; therefore Desbazeille et al. [19] have studied the torsional mode effects in a twenty-cylinder engine and developed an analytical model with flexible crankshaft for the misfire diagnosis. Moreover, some researchers [20-22] tried to detect the misfires via the angular acceleration of the engine block. Based on the block angular acceleration, the engine output torque can be calculated and the cylinder

pressure can be obtained as well. The variation in block angular acceleration can reflect whether there is a combustion fault occurring.

However, when these vibration-based techniques are applied to the engines in a real situation, the misfires cannot automatically be diagnosed from the analysed vibration signals. Artificial Neural Networks (ANNs) have been chosen as the basis for the next generation of diagnostic effort by the US Navy [23]. A number of researchers have also recommended the use of ANNs as a way of automating the diagnosis of machine faults, and in particular faults in rolling element bearings [24-31]. So ANNs should be a potential solution to the problem of automated diagnostics of different faults in IC engines. A critical issue with ANN applications in machine condition monitoring is the network training, and it not feasible or economical to experience a sufficient number of different actual faults, or generate them in seeded tests, to obtain sufficient experimental results for the network training. Simulation is proving to be a viable way of generating data to train neural networks to diagnose and make prognosis of faults in machines. In reference [32], the main examples given were for simulation of faults in gears and bearings in rotating machines. There was also a small section on faults in IC engines. Desbazeille et al. [19] also simulated the misfires in a large 20-cylinder diesel engine with flexible crankshaft as mentioned above.

In this paper, the measured torsional vibration of the crankshaft and the roll angular acceleration of the engine block are used for the diagnostics of misfires. An ANN based system was developed to automatically diagnose misfires in IC engines and includes three phases:

1. Identification of a fault condition, including fault type.
2. If a fault, which cylinder?
3. Given fault type and cylinder, what is the severity?

Multi-Layer Perceptron networks (MLPs) were used to detect whether there is a misifre (MLP1) and to identify the severity of misfire (MLP2). A Probabilistic Neural Network (PNN) was used to identify which cylinder has misfires. This paper embodies new developments and extensions of our former conference papers [33-35]. In our former works [33-35], we tried to use only one MLP (MLP2), with nonlinear log sigmoid transfer function, to identify the severity of the misfires at all speeds/loads, but homed in on the particular severities tested, so the nonlinear (stepped) output does not logically agree with the real situation of identification of continuous variations in the misfire severity, and the classification results are coarse. In this paper, separate MLPs with saturating linear transfer functions were introduced for the severity identification at each speed condition, and therefore the linear output can more accurately indicate the reality of a continuously varying (rather than stepped) condition, and the classification results can be much finer. In order to provide sufficient data for the training of the networks, simulation models were built to simulate different ranges of misfires. During the process of building the simulation models, based on a particular engine, some mechanical and physical parameters, for example the inertial properties of the engine parts and parameters of engine mounts, were first measured and calculated. The thermal and mechanical principles of IC engines were studied and incorporated into the models. The simulation models were also validated and updated by a series of experiments. Advanced digital signal processing techniques were applied to the experimental and simulated vibration signals. The input vectors to the ANNs were extracted/selected features from the processed signals. Finally, the ANN systems were trained using only the simulated data and tested using real experimental cases. Because the simulation models are based on the thermodynamic and mechanical principles of IC engines, the proposed diagnostic system can firstly be expected to be extended to a wider range of faults (in terms of location and severity) than those used to validate the model, and can in principle be adapted for any engine (once again with a relatively small number of validation tests).

2. Vibration measurement and signal processing

The premise of using simulation data to train the networks is that the simulation systems have to be updated and evaluated using at least a small number of experiments. Meanwhile, some mechanical and physical parameters are the required inputs for the simulation models, such as the inertia properties of the engine and its components and the parameters of the engine supports. Therefore the vibration based measurements, and signal processing techniques used are introduced first in this section.

2.1 Experimental set-up and data acquisition

A series of vibration signals in normal condition and with misfires and mechanical faults were recorded on a Toyota 3S-FE 4-cylinder gasoline engine at UNSW. The firing sequence of the engine is 1-3-4-2. The engine was connected to a hydraulic dynamometer which provided an external load. By controlling the dynamometer, three constant speed conditions were selected: 1500rpm, 2000rpm and 3000rpm. For each speed, there were three different load conditions: 50Nm, 80Nm, 110Nm. The injection and firing of the engine was managed by a special Engine Control Unit (ECU), of type Motec M800. Removing the ignition lead from the spark plug is the most direct way to simulate 100% misfire. By controlling the fuel injection quantity in the ECU control program, 50% misfire was also simulated experimentally on the engine.

The sampling frequency of the recording system was 25600 samples/s. The instruments for the vibration signal measurement include five accelerometers and two proximity transducers. The accelerometers were used to record the vibration on the surface of the engine block and their layout is shown in Figure 1(a). The proximity transducers were used to pick up a once-per-rev tacho signal and a ring gear encoder signal (tooth passage). For the once-per-rev pickup, a small piece of steel was glued onto the flywheel with its position corresponding to the top-dead-centre (TDC) of cylinder 1 (see Figure 1(b)). Because there are 120 teeth on the ring gear, that proximity probe records 120 pulses each revolution. Additionally, a pressure sensor, which is integrated with a spark plug, was used to measure the cylinder chamber pressure in one cylinder at a time. Some raw signals at 1500rpm/110Nm are shown in Figure 2. The *X*-axis is the time sample numbers, and the ring gear signal is zoomed in Figure 2. From the raw signal, it can be seen that the cylinder pressure in each cycle varies somewhat, so it is necessary to synchronously average the pressure signal to update the combustion chamber pressure of the simulation models in the simulation section of this paper. For each cycle, there are two tacho signals corresponding to the TDCs in the firing stroke and expansion stroke. But only the tacho signal in the firing stroke is useful for the fault diagnostics (especially for identifying the localization of faults). In the signal processing, the pressure signals in the cylinder 1 are close to the tacho signals in the firing strokes, so they were used to remove the tacho signals in the expansion strokes from the measured tacho signals. From the measured raw ring gear encoder signal, it can also be seen that there is small change of the absolute clearance between the tops of the teeth and the proximity probe, giving both a low frequency drift and an amplitude modulation. However, the amplitude fluctuation in the raw signal has no effect on the phase demodulation, since it is primarily the zero crossings which indicate the phase modulation (after removal of the low frequency drift). Note that the low frequency drift is automatically removed by the bandpass filtering used for the phase demodulation.

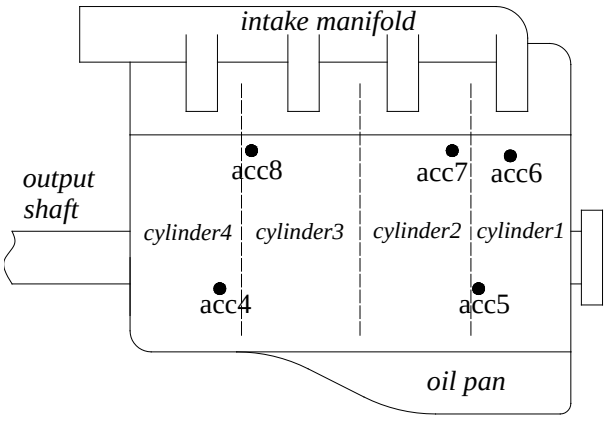

(a) accelerometers

(b) once-per-rev proximity transducer

Figure 1. Instrumentation layout.

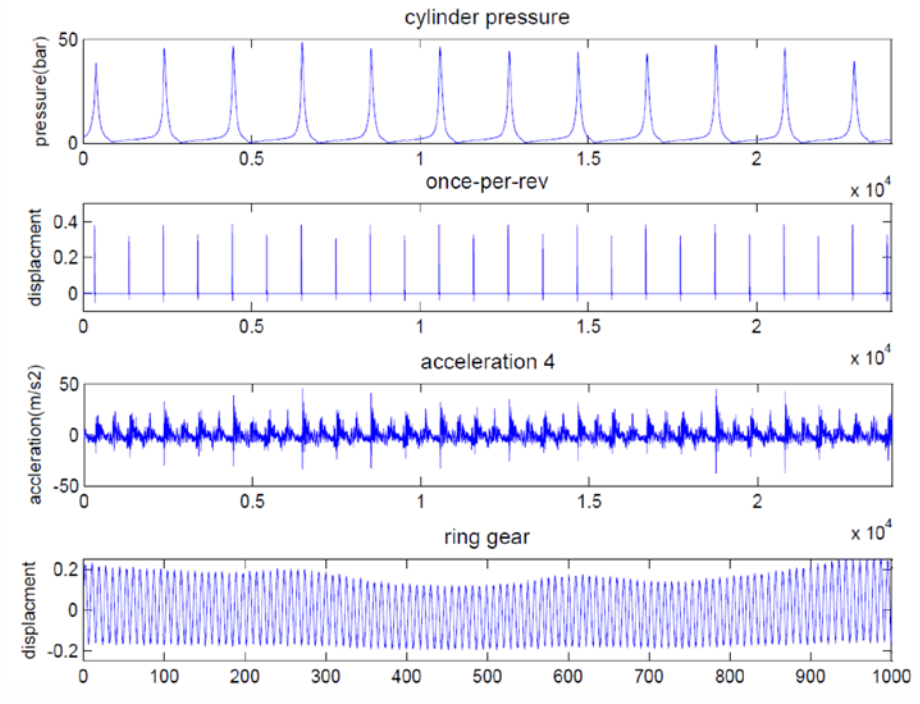

Figure 2. An example of raw measured signals

2.2 Torsional vibration for misfires

There are several approaches to recording torsional vibration signals. Janssens [36] compared the accuracy and performance of five measurement techniques, including a high-speed incremental encoder, dual beam laser interferometer, zebra tape, zebra disc and direct pulse measurements with magnetic probe. The most fundamental transducer for measuring torsional vibration is the incremental optical encoder. This device provides an electrical pulse train, where the time interval between successive pulses is inversely proportional to the average speed of the encoder shaft over each time interval. In recent years, the two-beam laser vibrometer has been used for the torsional vibration measurement, but the price is very high. On the other hand, the ring gear encoder signal is an economical and reliable method for torsional vibration measurement. Moreover, ring gear encoders measure the relative torsional vibration of the shaft to the block, which is most relevant here, whereas laser vibrometers measure the absolute torsional vibration, including rocking of the engine block.

For machine condition monitoring, torsional vibration signals can be considered as a phase modulated signal. It has been shown that phase demodulation can be a useful technique for diagnostics of rotating machines. McFadden [37] confirmed the importance of phase modulation in the early detection of fatigue cracks in gears. In order to diagnose the gear transmission error, Sweeney & Randall [38] examined the role of phase demodulation in the extraction of torsional vibration signals from encoder signals, where the transmission error is the differential scaled torsional vibration of the two gears. Sassi et al. [39] used the phase demodulated instantaneous angular speed to monitor the condition of electric motors. A phase modulated signal contains information in the variation of its phase. An example of a phase modulated signal, in its simplest form, is the phase of a single cosine function modulated by another cosine wave, such as:

$$x(t) = A\cos\left(\omega_0 t + \phi_0 + \beta\cos(\omega_1 t + \phi_1)\right) \tag{2-8}$$

Evidently, phase demodulation involves analysing a signal to characterise how the oscillating phase component $\beta\cos(\omega_1 t + \phi_1)$ of the modulated signal varies with time (around the linear change $\omega_0 t$ given by the carrier frequency component).

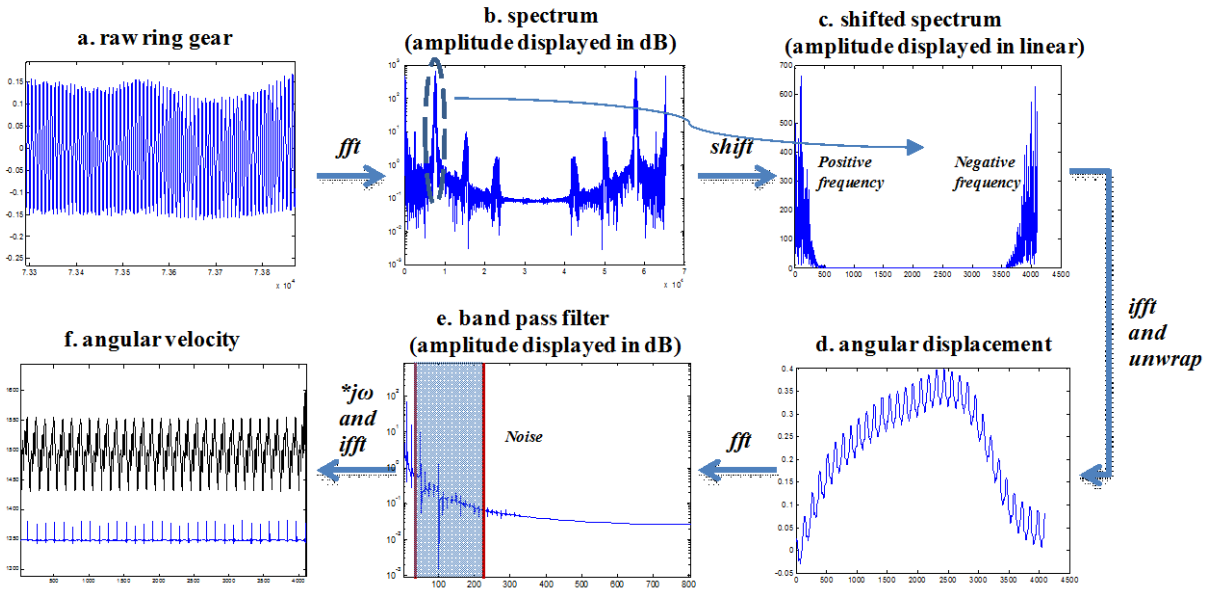

Figure 3. Phase and frequency demodulation of torsional vibration from encoder signal

The torsional vibration signal for the misfire diagnosis was obtained by phase demodulation of the ring gear encoder signal. Firstly, an FFT is performed on the encoder signal to get its complex spectrum. The amplitude of the complex spectrum can be displayed in dB as shown in Figure 3 (b), so that the frequency band which is to be demodulated can be determined and the width of band should contain all significant sidebands. Normally the first harmonic is selected. Because only the positive frequencies are selected, the demodulated frequency band is the spectrum of an analytic signal. The phase information will then be the angle defined by the real and imaginary components of the complex analytic signal. Next a new shifted spectrum of reduced size (4096 lines in this case) is set up and first filled with zeros, and then with the low positive frequencies taken from the encoder spectrum starting at the carrier frequency and with the significant (complex) samples to the right of it. The corresponding negative frequencies (located just below the sampling frequency at the right hand end of the buffer) are taken from the original spectrum to the left of the carrier frequency. This means that the carrier frequency has been set to zero, leaving only the modulation signal. The amplitude of the new shifted spectrum is shown in the Figure 3 (c). The new shifted spectrum is not the spectrum of an analytic signal any more, because it now has a negative frequency part. But the phase information still exists in the new complex shifted spectrum. The unwrapped phase angle demodulated from the shifted spectrum represents the torsional vibration signal of the crankshaft when divided by the number of teeth (120) to get it in terms of the angular displacement of the shaft (Figure 3 (d)). Finally the angular displacement of the shaft was differentiated to get the angular velocity (Figure 3 (f)). To avoid amplifying high frequency noise, the differentiation was done by a $j\omega$ operation in the frequency domain, with band limitation from 8Hz to 195Hz (Figure 3 (e)). In this way a bandpass filtered differentiated signal was formed in one operation.

Likewise, after performing an FFT on the tacho signal, a shifted spectrum of the same reduced size (4096 lines) was set up and its positive frequencies taken from the first 2048 lines of the tacho spectrum. Then performing an IFFT on the shifted spectrum and keeping the real part, finally we get new tacho signals, which have same sampling ratio as the calculated angular velocity. Therefore the torsional vibration in terms of degrees of crank angle is related to the tacho signal (360 degrees between two new tacho pulses), instead of the original sampling frequency of the recording system.

The demodulated synchronously averaged torsional vibrations under normal condition at 1500rpm but different loads are shown in Figure 4. The synchronous averaging is based on the TDC in the firing stroke of cylinder 1. Regarding the number of averages, if the signals were averaged over a certain period for two firing cycles, and there is no big difference between the two cycles of the averaged results, it means the number of averages is sufficient. For the convenience of the following processing, the two cycles were then averaged to give the final average over one firing cycle. It can be found that the torque contributions from each cylinder are more uniform at higher load conditions.

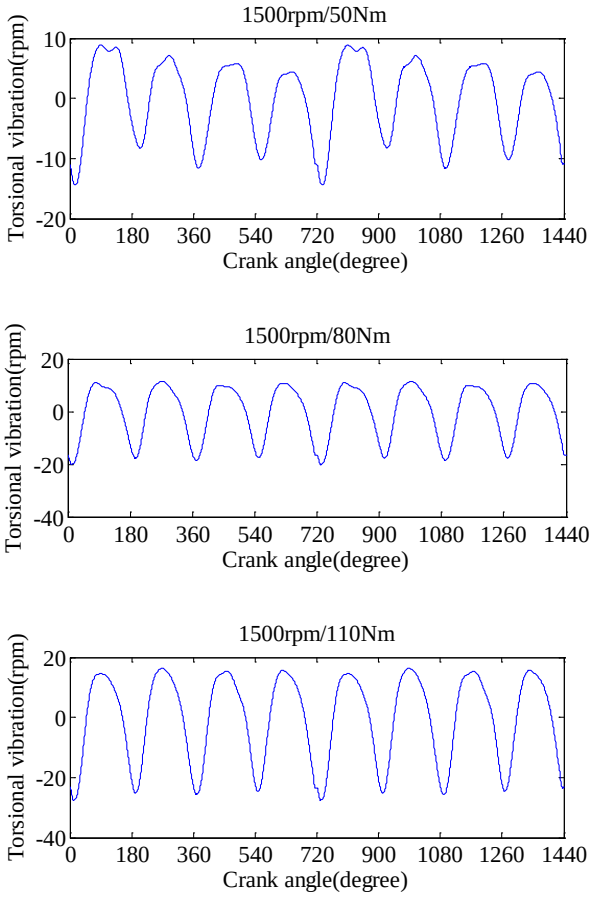

Figure 4. Torsional vibration under normal condition at 1500rpm but different loads

When misfire (100% misfire) occurs in cylinder 1, it is found that the overall waveforms of torsional vibration are very similar at any speed and load condition and overall waveforms can clearly indicate the existence of misfire (as shown in Figure 5). Based on the tacho signal, it is easy to identify which cylinder has a misfire.

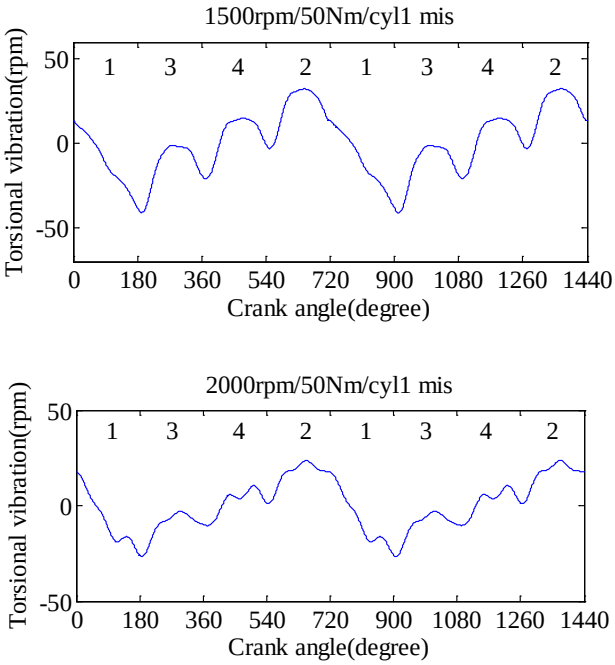

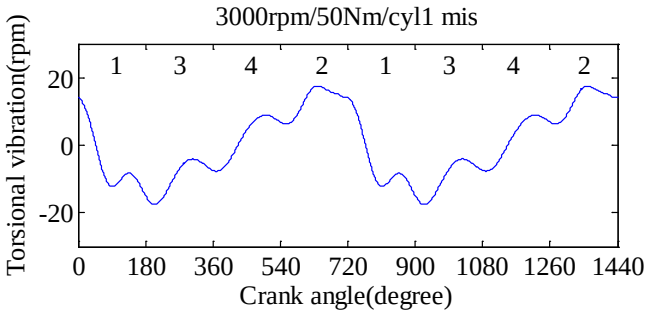

Figure 5. Torsional vibration for the 100% misfire in cylinder 1 at 50Nm but different speeds

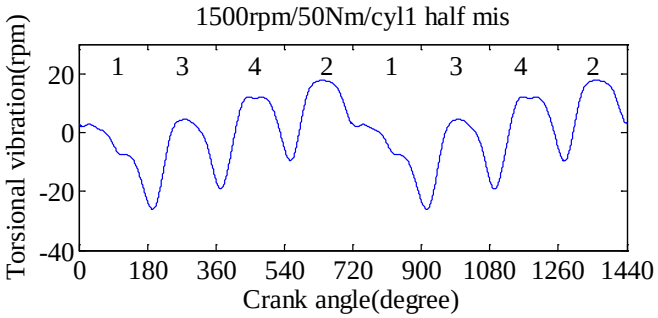

Figure 6. Torsional vibration with 50% misfire in the cylinder 1

It can be seen that the overall waveform of the torsional vibration signal with 50% misfire is very similar to those with 100% misfire and an example is shown in Figure 6.

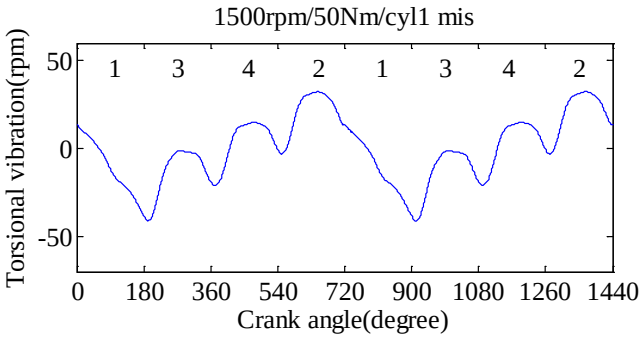

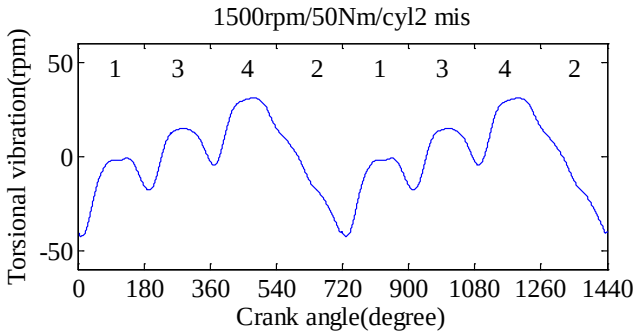

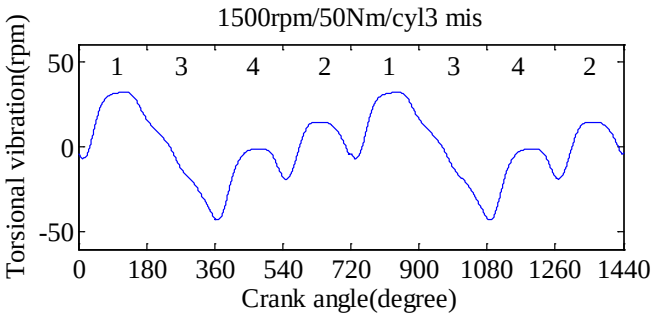

Figure 7. Torsional vibration with 100% misfires in different cylinders

As mentioned before, a misfire was also created in cylinders 2 and 3 (examples shown in Figure 7). Again, the overall waveforms with misfires in other cylinders are very similar to those with misfire in cylinder 1 (at any speed and load condition), only with phase shifts.

2.3 Pseudo angular acceleration of the engine block

The pseudo angular acceleration (roll rotation) of the engine block was estimated from the difference of a pair of acceleration signals. The signals from accelerometers 5 and 7 (Figure 1) were subtracted to remove the translational components. The subtraction results were divided by the distance between the two measurement points to calculate the pseudo angular acceleration of the block. It is called pseudo angular acceleration because the measurement points are not in line with the centre of gravity (CG) of the engine (which could not be determined exactly). Their line is not parallel to the principal axis of the engine either, so the calculated angular acceleration is mixed with other rotational motions.

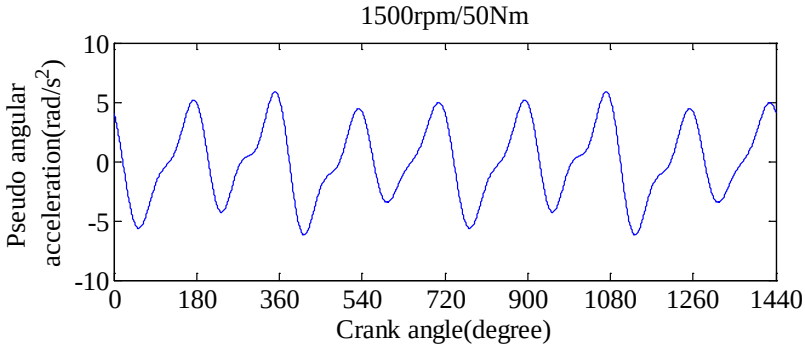

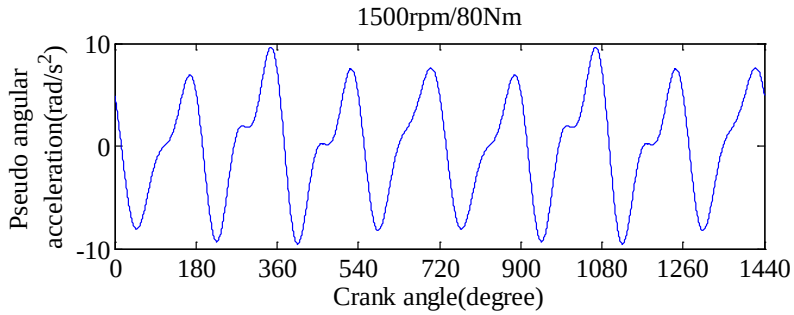

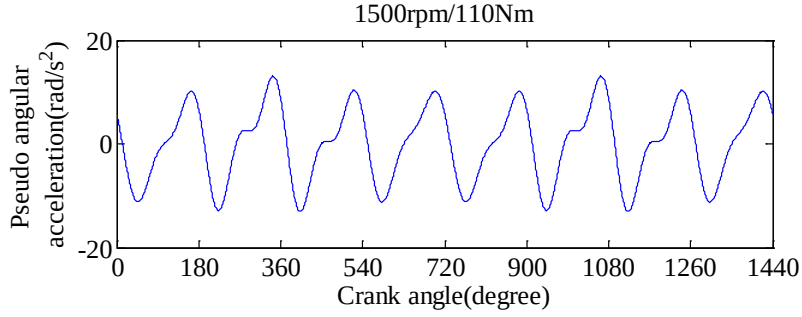

Figure 8. Pseudo angular acceleration under normal condition at 1500rpm but different loads

The firing frequency is quite low compared to the engine block structural resonances and is 100Hz for the highest speed in the experiments (3000rpm). Therefore, after the results of subtraction of pairs of accelerations were passed by a low-pass filter, the high frequency structural resonances were removed and the curve of pseudo angular acceleration became very clear. The pseudo angular accelerations in normal conditions at 1500rpm but different loads are shown in Figure 8. It is quite understandable that the fluctuation of pseudo angular accelerations increases at higher loads, because the excitation frequency is the same at the same engine speed, but higher output loads give rise to bigger excitation torques on the engine block.

Similar to the torsional vibration, when the engine operated at the same load but different speed (as shown in Figure 9), the torque balance from each cylinder deteriorated at higher speed.

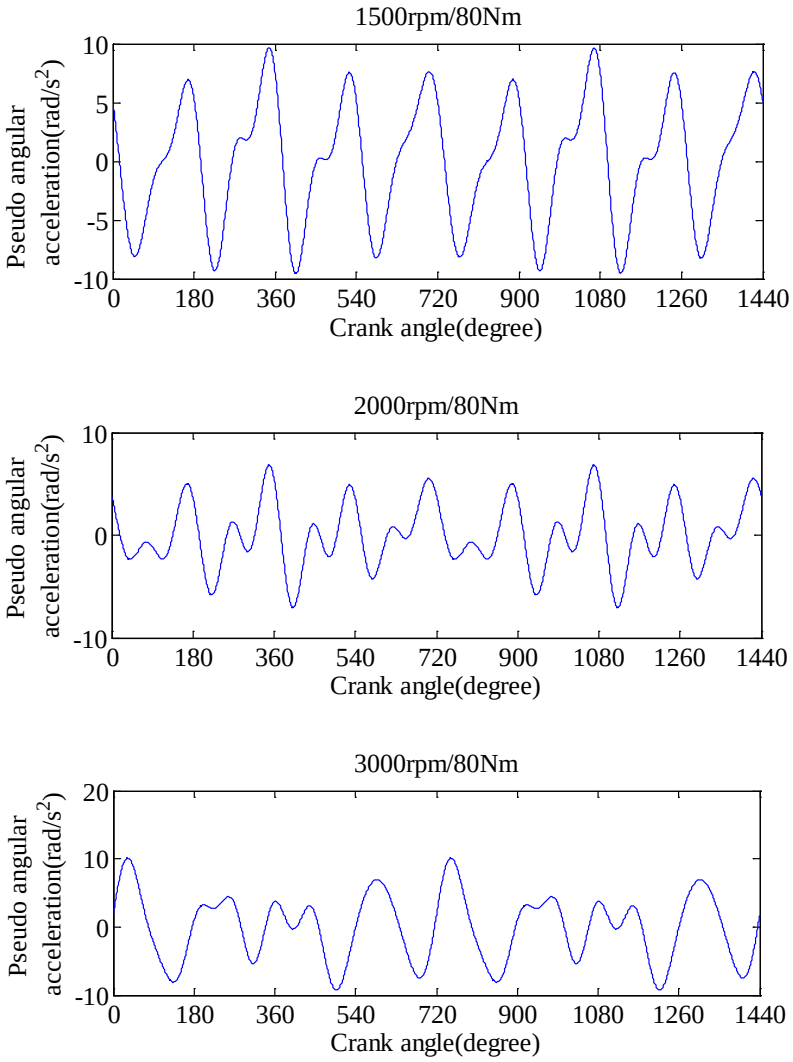

Figure 9. Pseudo angular acceleration under normal condition at 80Nm but different speeds

When 100% misfire occurs in cylinder 1, the overall waveforms of pseudo angular acceleration at the same speed (possibly with different load) are very similar, but the overall waveforms of pseudo angular acceleration at different speeds have visible changes (as shown in Figure 10). That is because the combustion force frequencies change at different engine speed. The frequency change of the force means that the response is associated with different sections of the Frequency Response Function (FRF) of the engine block rigid body modes (determined by the inertia properties of the engine and stiffness of the suspension system).

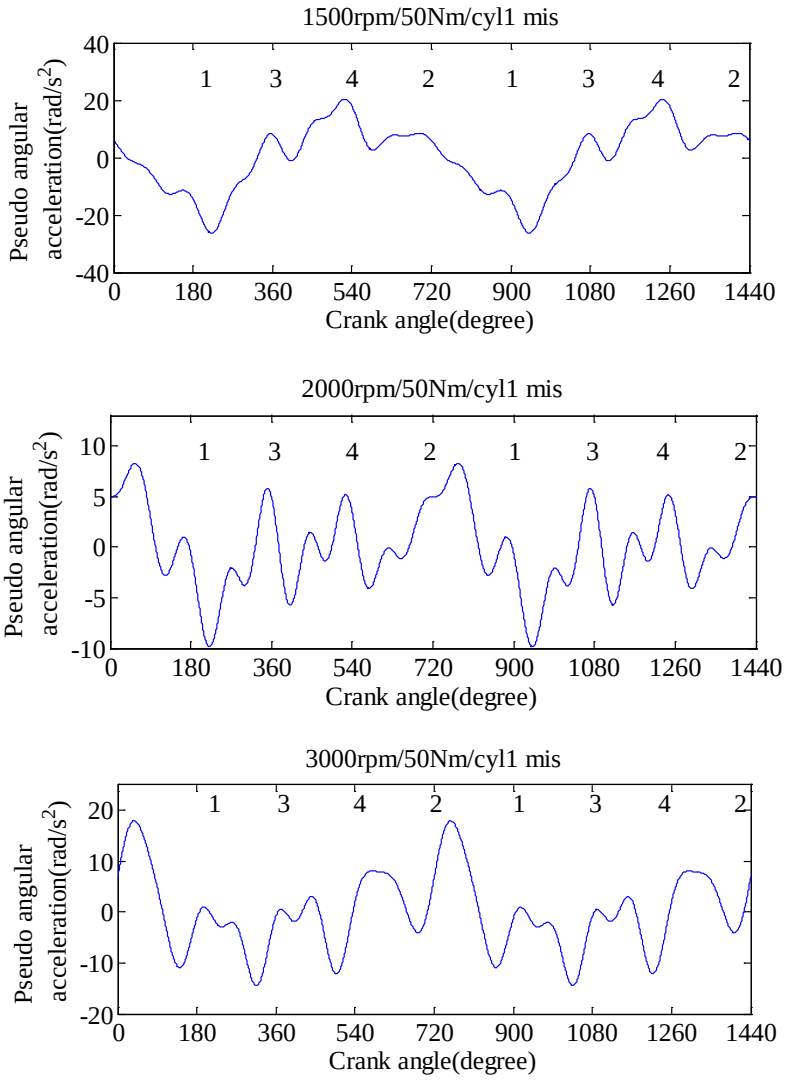

Figure 10. Pseudo angular acceleration with 100% misfire in cylinder 1 at 50Nm but different speeds

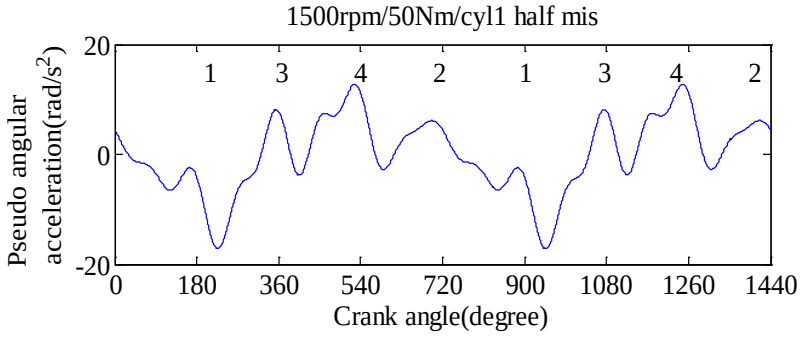

Figure 11. Pseudo angular acceleration with 50% misfire in cylinder 1

However, it can be seen that the overall waveform of the pseudo angular acceleration with 50% misfire is very similar to those with 100% misfire (at the same engine speed) and an example is shown in Figure 11.

When the misfire occurs in different cylinders at the same speed (the load can be different), the overall waveforms of the pseudo angular accelerations are very similar to those with misfires in cylinder 1, only with phase shifts (as shown in Figure 12).

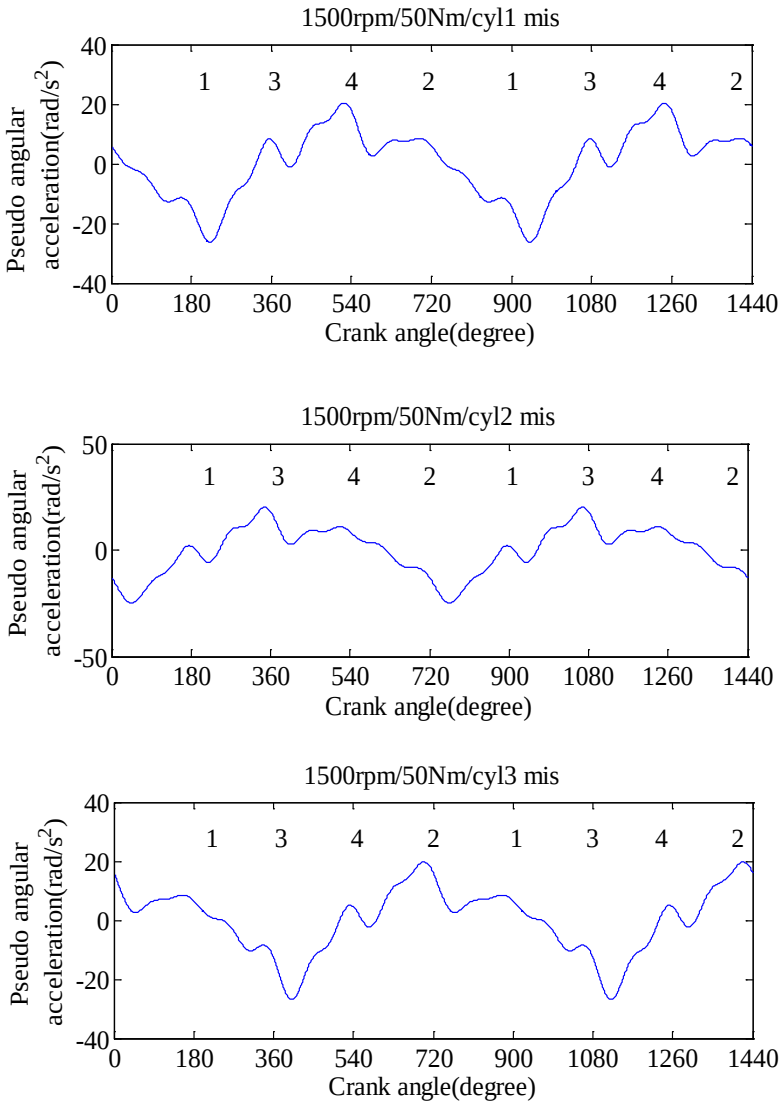

Figure 12. Pseudo angular acceleration with 100% misfire in different cylinders

Judging from the waveforms of the two approaches in normal and misfire condition, it can be concluded that the torsional vibration signal is easier and more straightforward to interpret than the block angular acceleration signal for misfire detection. That is because the block angular acceleration is subject to more influences, such as the interaction of varying frequency forcing functions with a fixed transfer function, and more additive noise. It should be remembered that the torsional vibration would have a fixed transfer function for a flexible crankshaft and the torsional modes will then affect the torsional vibration at different speeds, but because the experimental engine is a small four-cylinder engine, the flexible modes of the crankshaft are outside the range where they have a significant effect on the torsional vibration. In the misfire simulation model in the following section, the crankshaft was built as flexible and it was verified that the first flexible mode was much higher than the highest firing frequency in the experiments. If the torsional modes of the crankshaft were within the excitation range, as in the work of Desbazeille et al. [19], the torsional vibration approach would suffer from the same problems as the block angular acceleration with variation in speed. However, the block angular acceleration approach only relies on very low frequency information from a pair of acceleration signals, so it is feasible and reliable to use budget accelerometers to diagnose the misfire by this means (even though sophisticated and highly sensitive accelerometers were applied in the experiments).

2.4 Feature extraction and selection

The most important thing for the engine diagnosis is to find parameters to interpret the waveform fluctuations. With such parameters, the diagnosis system can automatically monitor the operation of any engine by pattern recognition technology. Therefore it is necessary to further analyse the waveform for

normal and misfire conditions in the frequency domain. Inspired by the pattern recognition research of Desbazeille et al. [19], polar diagrams were employed to interpret the harmonics of the waveform patterns from the processed vibration waveforms. The Fourier coefficients were studied and presented in polar diagrams. The amplitudes and phases of the first five harmonics were investigated for both the torsional vibration approach and the block angular acceleration approach. The polar diagrams with normal and misfire for two different speed/load conditions are shown in Figure 13. Because the Fourier transform interprets one cycle (two rotations) as 360º, the phase change of the 1st harmonic can be directly recognized in a 360 degree polar plot. The 4th harmonic represents the firing frequency. In the normal condition, the torque contribution from each cylinder is nearly uniform, so the amplitude of the 4th harmonic is most dominant. However in the misfire condition, it was found that the amplitude of the 1st harmonic (cycle frequency) became dominant. It was also found that the phases of the 1st harmonic for misfire conditions are nearly fixed.

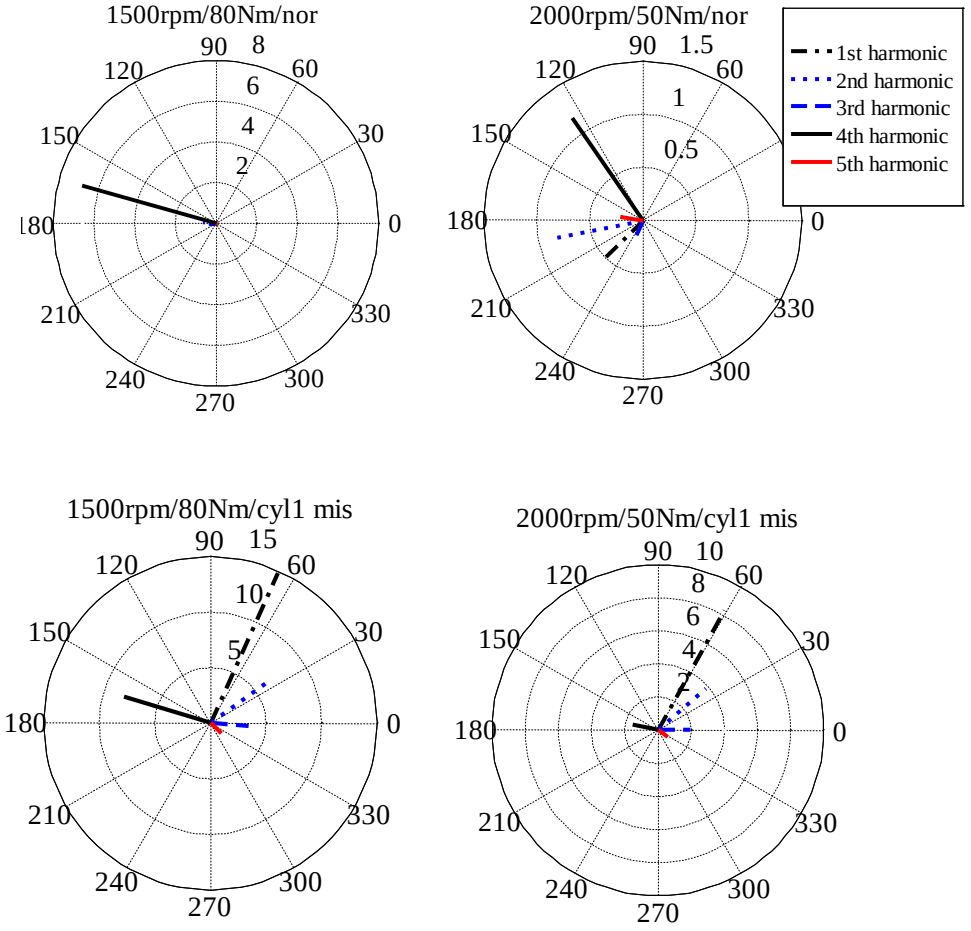

Figure 13. Polar diagram of torsional vibrations with normal and misfire conditions

The polar diagram for the torsional vibration waveform with misfire in different cylinders at 1500rpm/50Nm is shown in Figure 14. As mentioned before, because the Fourier transform interprets one cycle (two rotations) as 360°, it can be seen that the phase of the misfire in cylinder 1 is 90º ahead of the phase of the misfire in cylinder 3 instead of 180º (firing sequence is 1-3-4-2). Likewise, for the misfire in cylinder 2, there is a 270º phase lag behind the misfire in cylinder 1. So for a four-cylinder engine, there is 90 degree difference for the misfires in individual cylinders (60 degree difference for a six-cylinder engine).

A conclusion for the misfire diagnosis is that the amplitude ratio of the 1st harmonic to the 4th harmonic of the torsional vibration can be a good feature for the detection of misfire and the phase of the 1st harmonic can be used for identifying the location of the misfire. It is worth pointing out that because the 4th harmonic indicates the firing frequency, the phases of the 4th harmonic cannot be used to identify the localization of

the misfires (for the misfire in individual cylinders, when the 90 degree difference of the 1st harmonic is multiplied by 4, it is 360 degrees and phase differences will disappear).

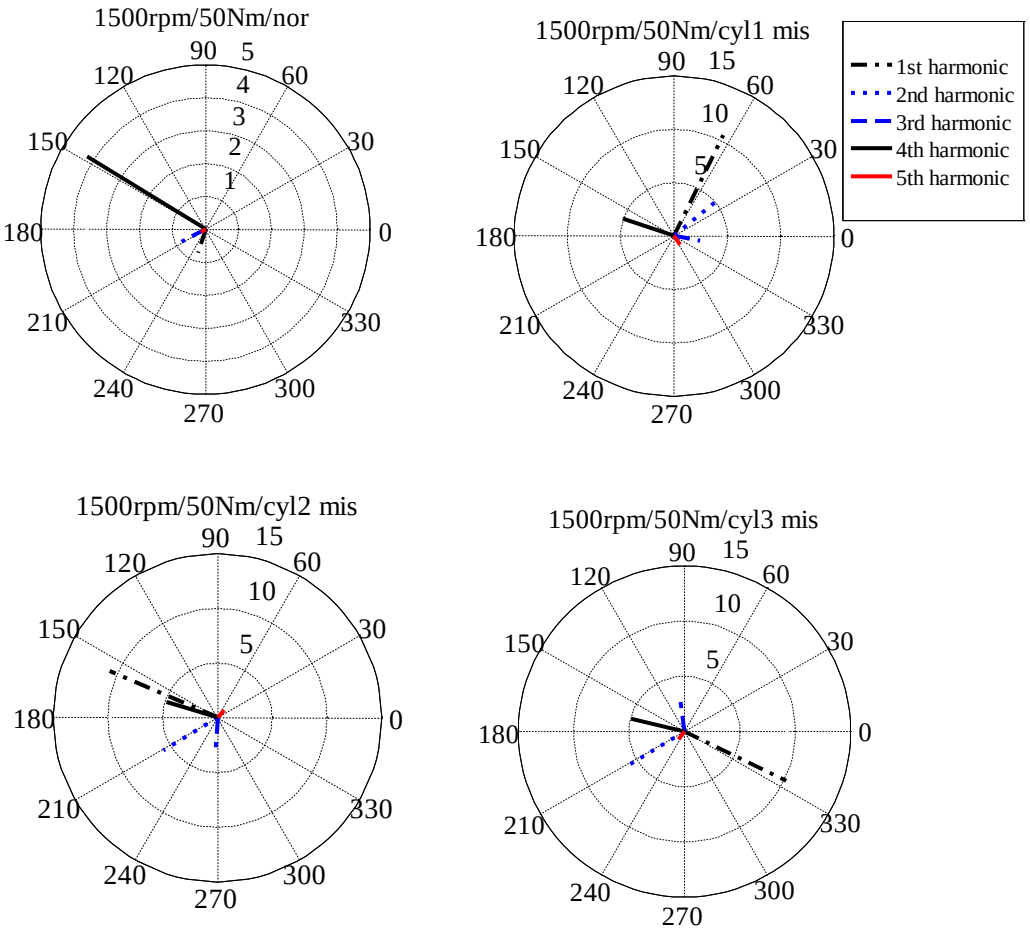

Figure 14. Polar diagram of torsional vibrations with misfire in different cylinders

Likewise, the polar diagrams of the block angular acceleration for normal and misfire conditions are shown in Figure 15. Compared to the polar diagram for torsional vibration, the amplitude of the 1st harmonic in the misfire condition is not dominant, but the amplitude increase of the 1st harmonic from normal condition is quite obvious. The amplitude ratio of the 1st to the 4th harmonics is still a good potential feature for the misfire detection.

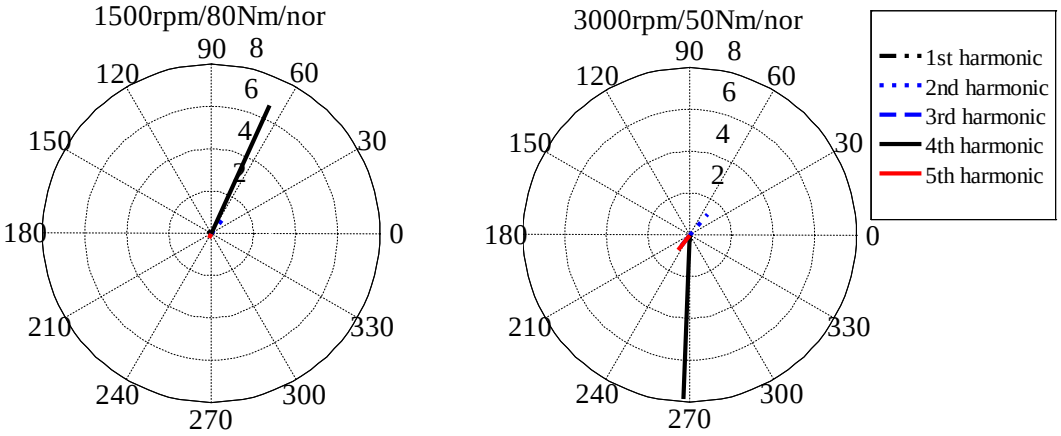

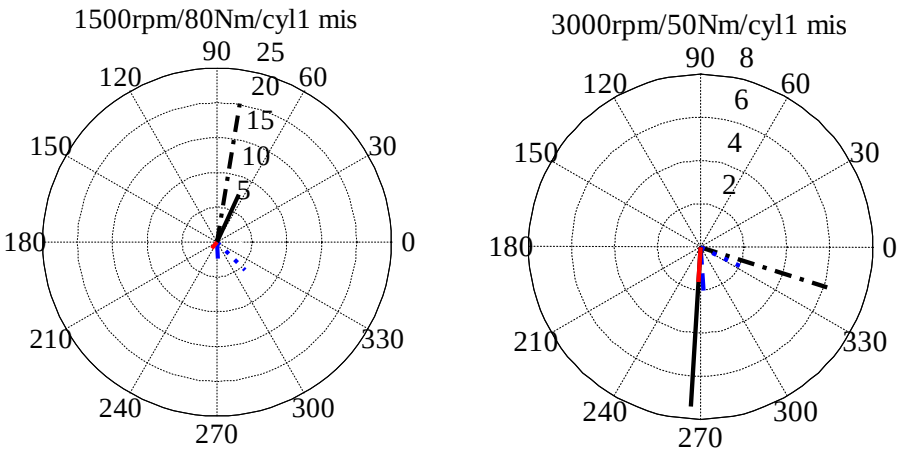

Figure 15. Polar diagram of block angular accelerations with normal and misfire conditions

From Figure 15, it can be seen that at the different speeds/loads, the phase of the 1st harmonic for misfire condition is not fixed. As mentioned before, that is because the combustion forcing frequencies change at different engine speed. On the other hand, the frequencies of the rigid body modes of the engine block remain fixed. Therefore, using the phase change of the 1st harmonic to determine which cylinder has a misfire is not straightforward as for torsional vibration (with effectively rigid crankshaft). But if the polar diagram at the same speed is considered, it can be found that the phase of the 1st harmonic with misfire is nearly fixed. As shown in Figure 16, there is a 90 degree difference for misfire happening in different cylinders as expected (likewise, there would be 60 degree difference for a six-cylinder engine). Therefore, the phase of the 1st harmonic can also be used for the misfire localization in the diagnosis process, but the engine speed should be taken into account.

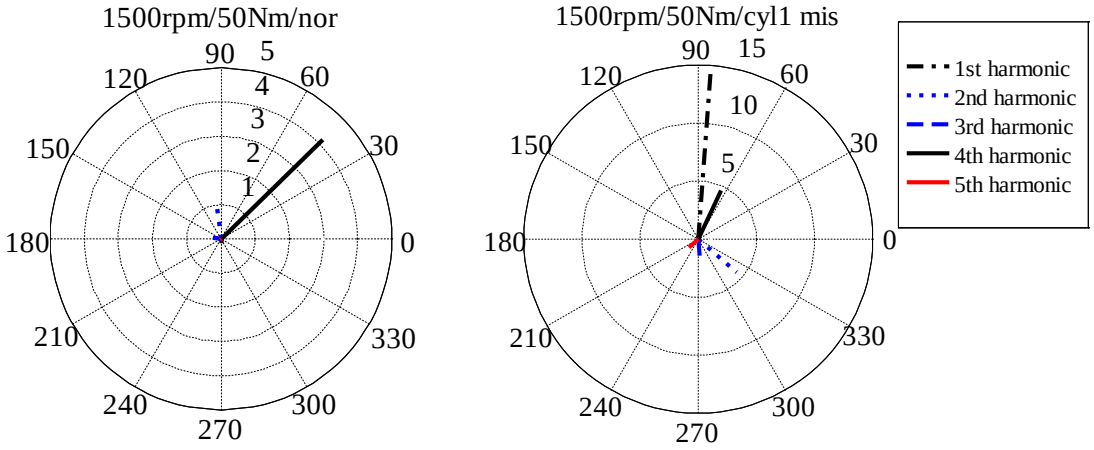

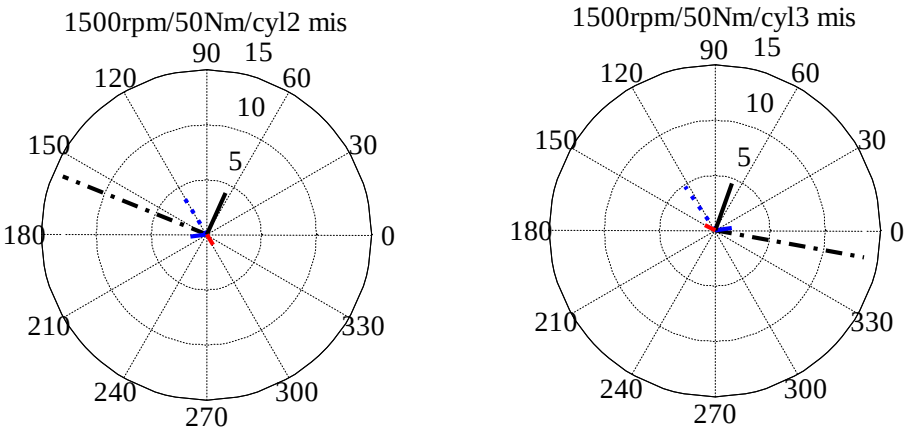

Figure 16. Polar diagram of block angular accelerations with misfire in different cylinders

It can be seen that the polar diagram can give more concise information than the waveform for the pattern recognition. After the amplitude and phase of the first five harmonics were studied, it was found that the amplitude ratio of the 1st harmonic to the 4th harmonic can be used for the misfire detection and the phase of the 1st harmonic can be used for the misfire localization. The polar diagrams of both the torsional vibration approach and the block angular acceleration approach can indicate clear changes between normal and misfire conditions.

2.5 Inertial properties and rigid body mode tests

From the mechanical viewpoint, to generate and evaluate these models, the parameters of the engine components should be measured or calculated first. It is not difficult to get some parameters from direct measurements, such as the cylinder bore and the length of connecting rod. But the inertia properties of the components and the characteristics of the engine supports involve more complicated measurement and calculation. For the components with simple geometry, the inertia properties can be calculated using 3D CAD software. But for the complicated components, it is difficult to obtain accurate models in this way, so the calculated inertial properties are not accurate either. In recent years, some new vibration based methods have been developed to identify the rigid body properties of complex objects. These methods can be generally classified into two groups: the mass line method and the modal property method. Both of the methods start with artificially excited vibration data and their inputs are normally FRFs. The inertia properties of a measured object can be derived from the flat mass line or the rigid body modes.

In order to get accurate results, the two methods have different requirements on the suspension. The mass line method needs “soft” suspension to get clear mass lines but the modal property method needs a little stiffer suspension (compared to the suspension for the mass line method) to get separated individual rigid body modes. The mass line method has been widely studied [40-44] and successfully integrated into some commercial software, such as the “Rigid Body Calculator” in LMS Test.Lab. Based on the selected section of a mass line, the inertia properties can be solved from an over-determined set of equations by the least-squares method. The modal property method derives inertia properties from the analysed rigid body modes and mode shapes. Moreover, the modal property method is based on the rigid body modes so it is the only method that can solve for the corresponding stiffness and damping matrices from the measured vibration data. The details of this method can be found in [45-47]. As discussed in the preceding section, the rotations of the engine block (pseudo angular acceleration) were used for misfire diagnosis in this paper. In order to simulate the rotational motion of the engine block under normal and misfire conditions, the parameters of the engine suspension were extracted by the modal property method.

For the mass line experiment on the inertia properties of the whole engine, the whole engine was suspended by bungee cords and the point of origin for the measurements was taken as the output end of the crankshaft. The coordinate axes of the measurements are shown in Figure 17.

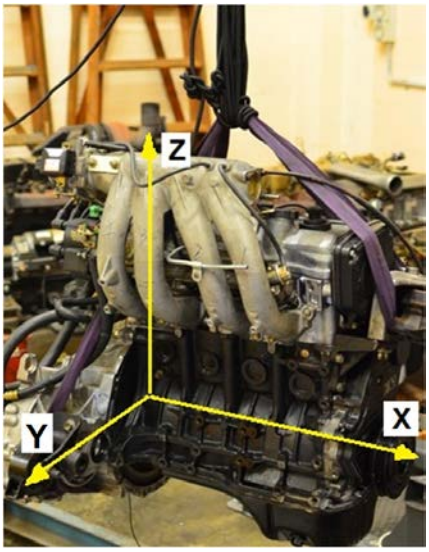

Figure 17. Inertial property measurement of the whole engine in the free-free condition

As mentioned before, the modal property method is the only method that can extract the parameters of the engine supports. As shown in Figure 18, externally excited vibration data (using an electrodynamic shaker, indicated in the red circle in the figure) was measured on the engine which was set on the engine mounts. There are 7 excitation DOFs and 21 measurement DOFs (including 7 driving point measurements).

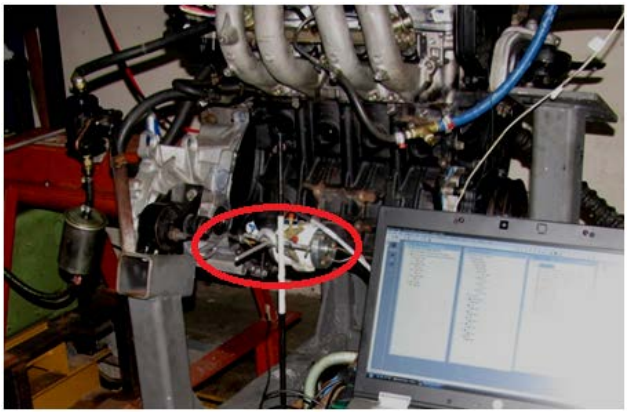

Figure 18. Vibration measurements of whole engine on the mounts

The details of the calculation of the parameters of the engine supports can be obtained from our former work [48]. It is worth pointing out that the calculation of stiffness and damping coefficients is quite challenging, especially for the damping. The engine mounts were considered as linear in the calculation, but this is not true in reality. The boundary conditions of the engine on the test rig are quite complicated, including the universal joint of the output shaft, inlet and outlet manifold connections and coolant hose connections. But overall the calculated stiffness and damping coefficients were found to be reasonable and rational. Moreover, the most important thing for the simulation of roll motion of the engine is to get good accuracy for the rolling rotation mode. As part of the simulation in the following section, the inertia properties and the parameters of the engine mounts were also further adjusted to get a better match between the simulation data and the experimental data.

3. Simulation of Misfires

3.1 Mechanical principles

The fundamental equation of the torque balance for an operating engine with rigid crankshaft is derived from the Lagrange formulation [8]:

$$I(\theta)\cdot\ddot{\theta}+\frac{1}{2}\cdot\frac{\partial I(\theta)}{\partial\theta}\cdot\dot{\theta}^2=T_g+T_{fric}+T_{load} \quad (1)$$

$$T_g=F_g(R\cos\theta\tan\phi-R\sin\theta) \quad (2)$$

All inertia related items are on the left side of Equation (1) and all the physically applied torques are on the right side. *I(θ)* is the polar moment of inertia about the crankshaft axis, and θ is the crank angle. On the right hand side of the equation, T_g is the torque contributed by combustion, T_{fric} is the friction and pumping torque of the engine, T_{load} is the external load imposed on the engine. In Equation (2), R is the crank radius, F_g is the combustion force and ϕ is the connecting rod angle. The torsional velocity $\dot{\theta}$ is one output of the simulation model. In order to simulate the misfire phenomena under various speed/load conditions, the most critical variable, cylinder pressure, should be first calculated.

The simulation of crankshaft torsional vibration is based on Equation (1), but the simulation of angular acceleration of the engine block is based on the moments/torques on the engine block about the crankshaft axes. The moments on the engine block by a single cylinder can be calculated from [49]:

$$T_{bk}=\frac{[F_g-m_pR\omega^2(\cos\theta+\frac{R}{b}\cos 2\theta)]\cdot\frac{R}{b}\sin\theta}{\sqrt{1+(\frac{R}{b}\sin\theta)^2}}\cdot(R\cos\theta-b\cos\phi) \quad (3)$$

F_g is the force from combustion, and ω is the rotating speed of the crankshaft. If misfires cause a change in the combustion pressure, according to Equations (1) and (3), the fluctuations of the torsional velocity and the pseudo angular acceleration of engine block can be observed in the simulations.

3.2 Cylinder pressure simulation

The compression pressure can be derived from the polytropic formula and the combustion pressure can be calculated by classic Wiebe's functions [50]. The details of pressure calculation can be obtained from our previous work [33-35, 51]. By multiplying the fuel injection quantity by a given percentage, the cylinder pressure under different misfire conditions can be simulated. The cylinder simulation model was also updated by the averaged measured pressure from the experiments. Normal, 50% misfire and 100% misfire conditions were simulated for different speed/load ranges. The pressure curves for normal, 50% misfire and 100% misfire in one cylinder at 1500rpm/80Nm are shown in Figure 19.

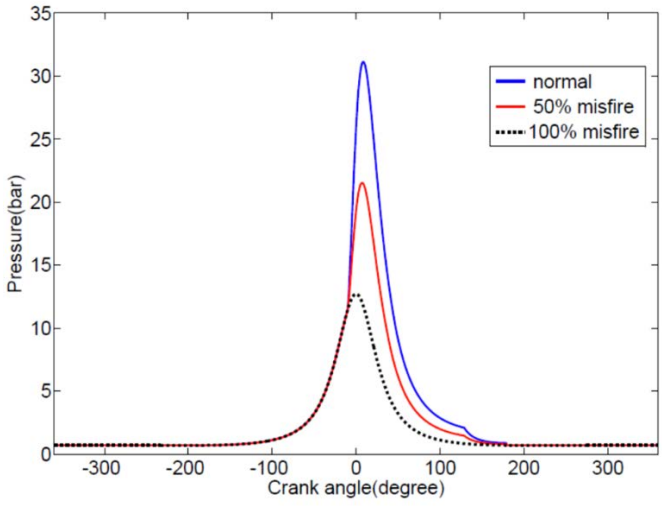

Figure 19. Pressure curves for normal and misfire conditions.

3.3 Torsional vibration simulation

The torsional vibration was initially simulated in the LMS AMESim package. The main components for the torsional vibration simulation are crankshaft/piston components and rotary spring and damper components. The crankshaft/piston components were connected by the rotary spring and damper components. The torsional damping coefficients of IC engines were estimated by the empirical determinations from Den Hartog [52] and Ker Wilson [53]. The torsional stiffness of the crankshaft was calculated in ANSYS. Ideally, the torsional stiffness should be calculated using the selected section shown in Figure 20. The forces/moments from two adjacent cylinders act on two half-sections of crank journals, then the angular displacement with respect to the journal bearings can be calculated, finally the torsional stiffness can be obtained. But in reality the central planes of the main journals can only rotate around the shaft axis (the *X* axis shown in Figure 20), with no translational movements in the *Y* and *Z* directions. It would be difficult to constrain the central plane of the crank journal in the model. However, most rotational deformations should come from the main journals instead of the crank web parts. As an alternative approach, two half-sections of main journals, two crank webs and one whole crank journal were selected and modelled in ANSYS, rather than one whole main journal, two crank webs and two half-section crank journals (as shown in Figure 21). The two central planes of the main journals were fixed in the modelling (based on considerations of symmetry).

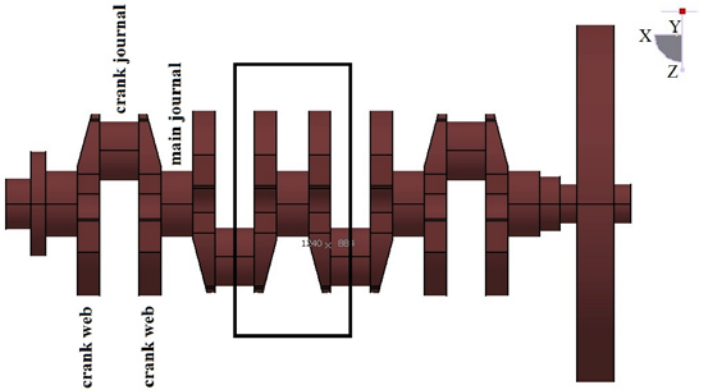

Figure 20. Ideally truncated section for torsional stiffness calculation

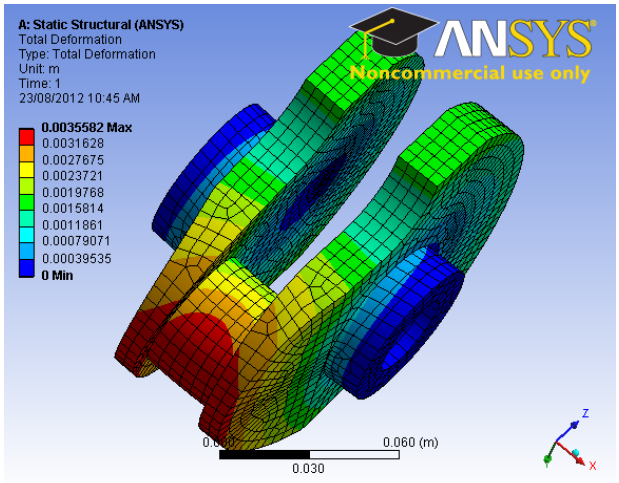

Figure 21. Torsional stiffness calculation model in ANSYS

A pressure force *p* was applied to the projection of the half cylindrical surface of the crank journal, and the torsional stiffness can be calculated by:

$$K_t = \frac{pAR^2}{4x_{cd}} \tag{4}$$

where A is the projected area of the cylindrical surface (length × diameter), R is the radius of the crankshaft (between main and crank journal centres) and x_{cd} is the deformation at the centre point of the crank journal.

The Toyota 3S-FE engine is small four-cylinder engine and it can be imagined that the crankshaft is quite rigid, but the effects of torsional modes on the torsional vibration still need to be checked. In the simulation model of AMESim, it was found that the lowest torsional mode is at 809.4Hz which is much higher than the highest firing frequency in the experiments (100Hz) so it gives the conclusion that the effects of torsional modes on the torsional vibration are very small. On the other hand, because the individual cylinders are connected by the rotary spring and damper units, the simulation model could easily be extended to the torsional simulation of larger engines, such as the 20-cylinder engine studied by Desbazeille et al. [19].

As mentioned in the preceding section, the torsional vibration was measured using the ring gear encoder. As opposed to a two beam laser vibrometer, which measures the absolute torsional vibration, the ring gear encoder measures the relative torsional vibration. However, the simulation model for the torsional vibration simulated the absolute torsional vibration rather than the relative torsional vibration. Therefore it is necessary to check the difference between the relative torsional vibration and the absolute torsional vibration. The relative torsional vibration should equal the absolute torsional vibration minus the rotation of the engine block. The rotational velocities of the engine block are simulated in the following section. It will be found that the angular velocities of the engine block are from 0.5-1 rpm, which is small in comparison with the torsional vibration velocity, normally around 10-20 rpm. Therefore, the conclusion is obtained that the simulated torsional vibration is roughly equal to the experimental torsional vibration.

The experimental torsional vibration signals and the simulated results for normal conditions are shown in Figure 22 for comparison. For the experimental torsional vibration at 3000rpm (shown in the Figure 22), even though the signal was synchronously averaged, the angular velocity wave for each cylinder is not uniform. That's mainly because the fuel injection and combustion is not balanced for the four cylinders at higher speed under the control of the ECU.

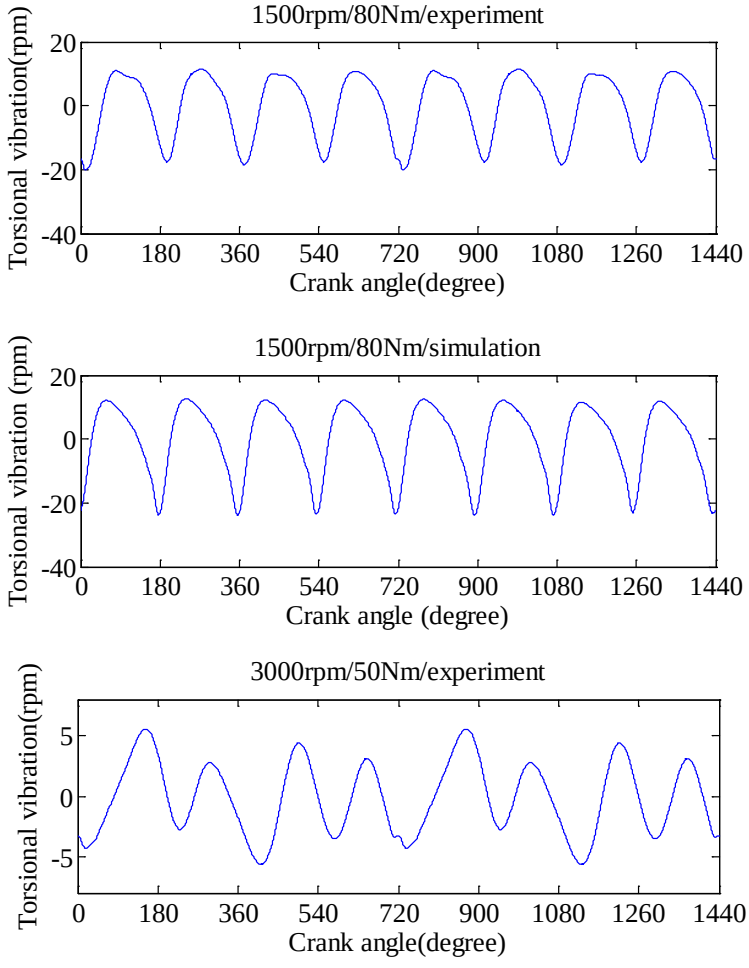

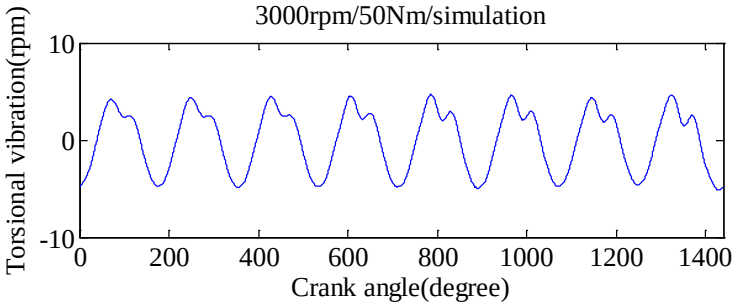

Figure 22. Experimental and simulated torsional vibration under normal conditions

After the simulation models were updated for normal conditions, the misfire conditions were simulated and the results were compared as well. Examples for the misfires happening in cylinder 1 at 1500rpm/80Nm and 3000rpm/50Nm are shown in Figure 23. It can be found that the simulated waveforms for the misfires showed a relatively good correspondence with those from the experiments.

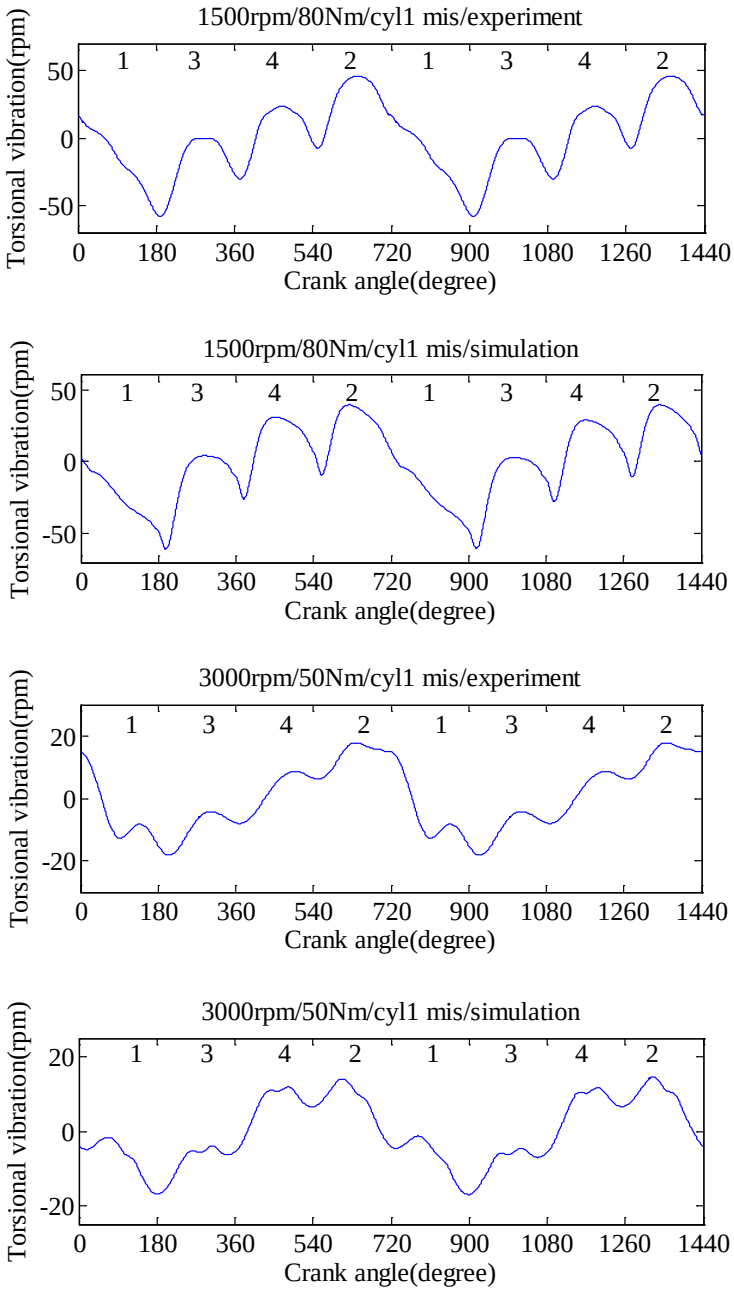

Figure 23. Experimental and simulated torsional vibration for the misfires in the cylinder 1

The 50% misfire at 1500rpm was also simulated and an example of the comparison of experimental and simulated waveforms is shown in Figure 24. It also gave a good match between the two waveforms.

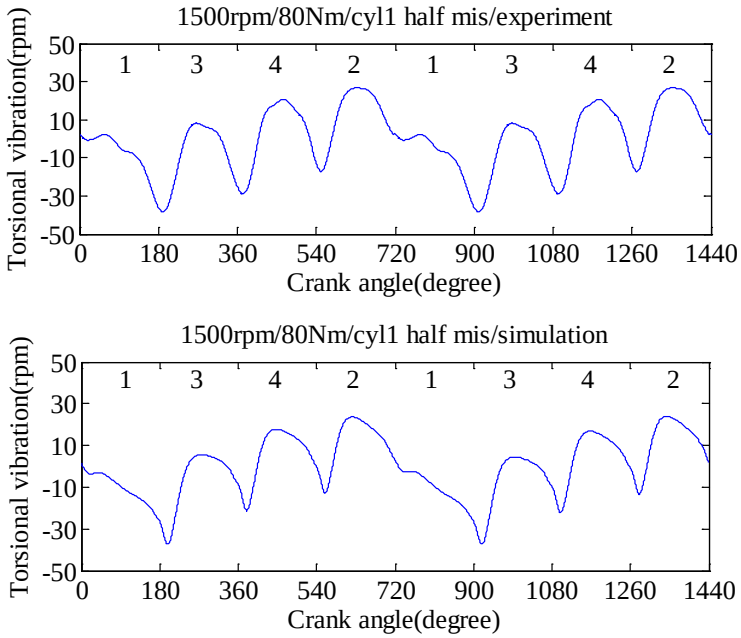

Figure 24. Experimental and simulated torsional vibration for the 50% misfires in the cylinder 1

As found in the preceding section, because the crankshaft is quite rigid and the effects of the torsional modes on the torsional vibration are very small, the simulated waveforms with misfires in the other cylinders are very similar to those for the misfire in cylinder 1, only with phase shifts.

The polar diagrams from simulated torsional vibration were also studied and two examples at 1500rpm/80Nm and 3000rpm/50Nm are shown in Figure 25. As discussed in the preceding section, the most useful information for the misfire diagnosis from the torsional vibration is the ratio of the amplitudes of the 1st and 4th harmonics and the phase of the 1st harmonic. From the Figure 25, it can be seen that this most useful information was simulated well. Overall, the simulated torsional vibration gave good matches with the experimental results, including both the waveforms and the polar diagrams. The simulation results can thus be used as the inputs to ANNs to train the automated misfire diagnosis system and the details are discussed in following section.

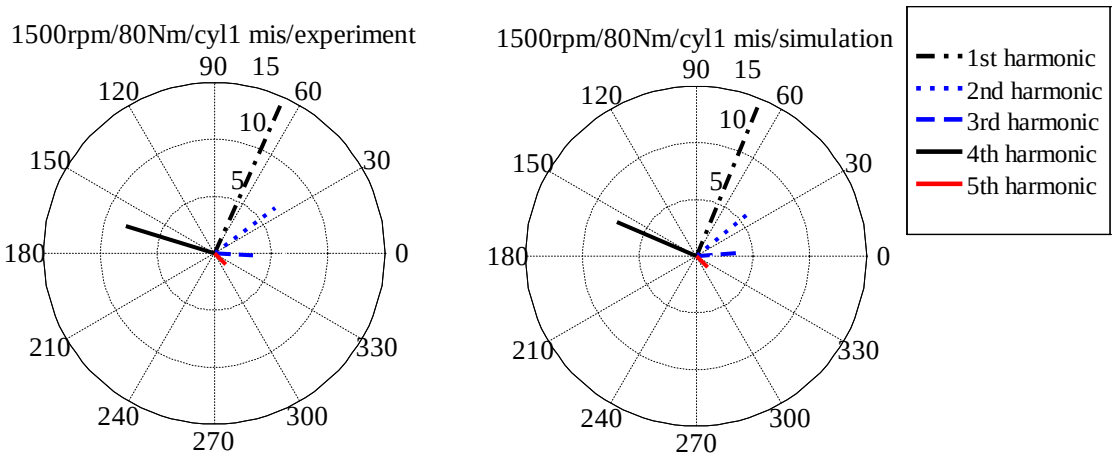

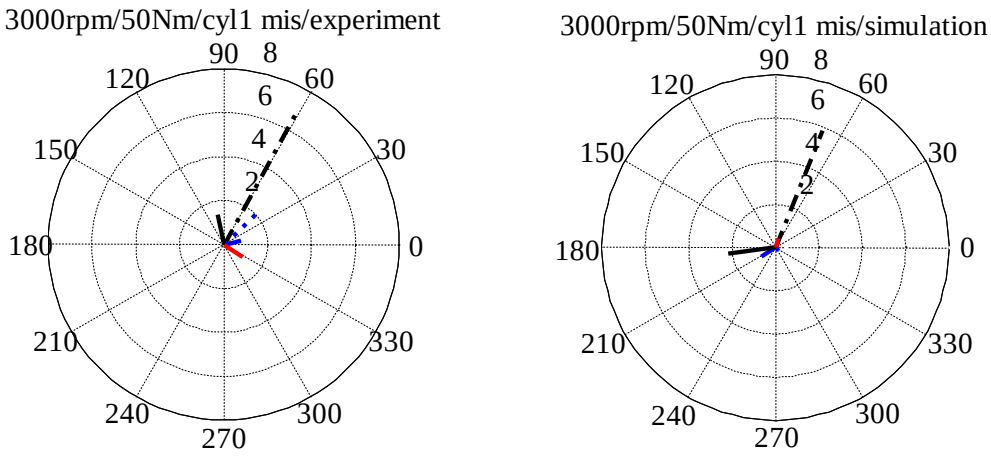

Figure 25. Polar diagrams of the experimental and simulated torsional vibration for the misfires in cylinder 1

3.4.Simulation of engine block angular acceleration

The simulation model of the engine block angular acceleration was also built in the LMS AMESim software package. The main components for the simulation of the angular acceleration of the engine block are crankshaft/piston model, 3D engine model and engine mount model. In the simulation model, the simulated angular acceleration of the engine block is about the CG of the engine and it is a genuine angular acceleration. In order to compare with the experimental pseudo angular accelerations of the block, the accelerations at the measurement points were first calculated, then the corresponding simulated pseudo angular accelerations were calculated.

During the simulation, the inertia properties and the parameters of the engine mounts were further adjusted manually to improve the match between the simulation data and the experimental data. The adjustments were based on the experimental results under normal conditions. Two examples of experimental results and the equivalent simulated results under normal conditions are shown in Figure 26.

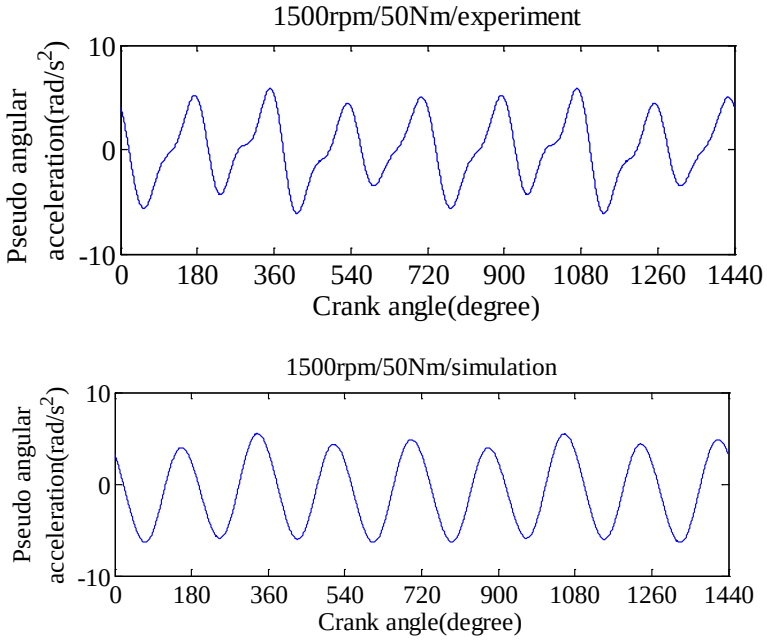

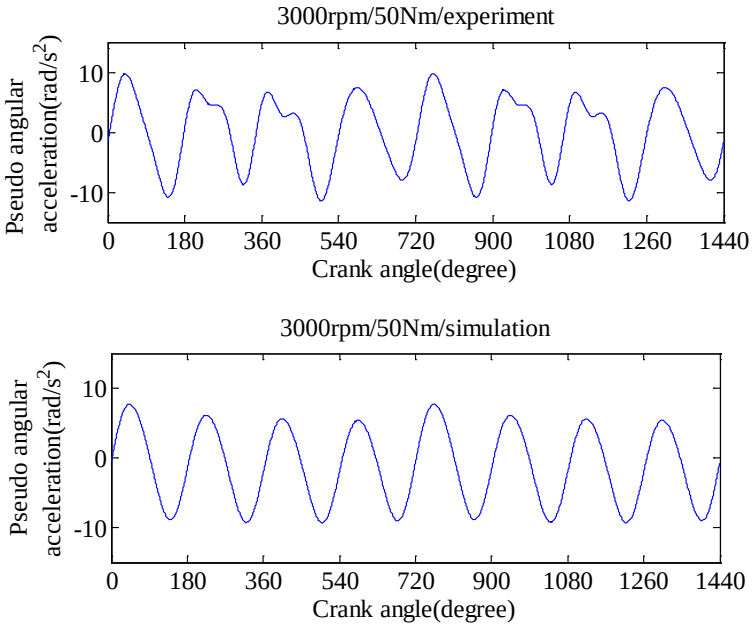

Figure 26. Experimental and simulated pseudo angular accelerations of engine block under normal conditions

Based on the updated model under normal conditions, the signals for the misfire conditions were simulated and these results were also compared with those from the experiments. Example results for the misfires happening in cylinder 1 at 1500rpm/50Nm and 3000rpm/50Nm are shown in Figure 27. It can be found that the simulated waveforms show good agreement with those from the experiments. Very similar to the case of simulated torsional vibration, when the misfire happens in other cylinders, the waveforms of pseudo angular accelerations of the engine block are nearly the same as those for the misfire in cylinder 1 at a certain speed, only with phase shifts.

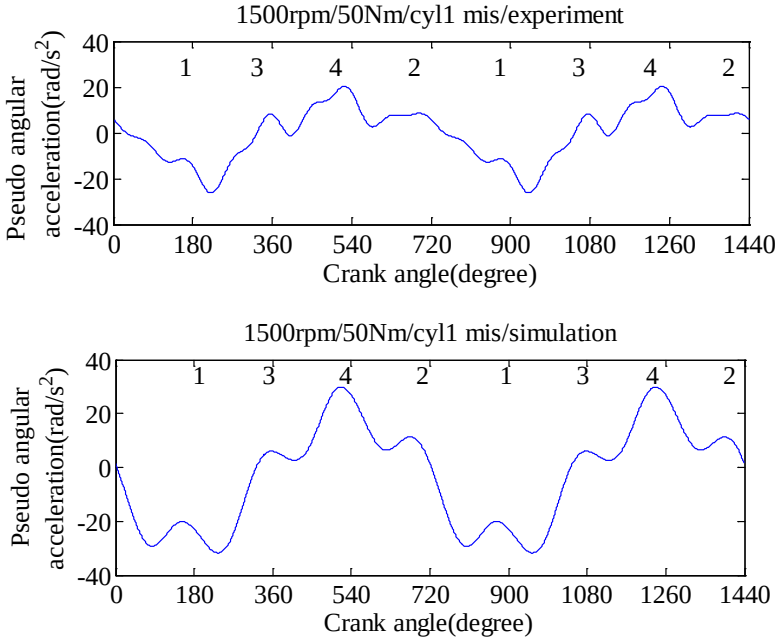

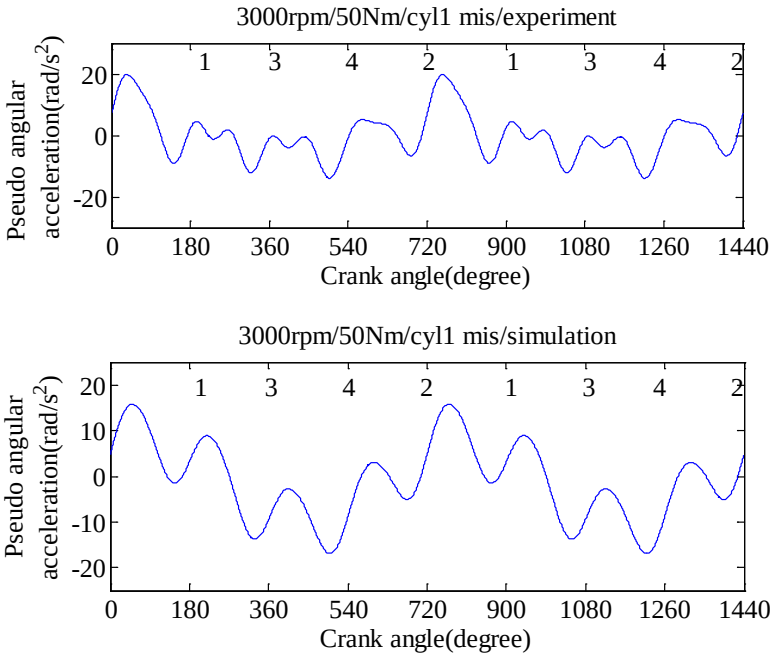

Figure 27. Experimental and simulated pseudo angular accelerations of the engine block for the misfires in cylinder 1

Likewise, the 50% misfires in cylinder 1 at 1500rpm were simulated and an example at 1500rpm/50Nm is shown in Figure 28. It can be seen that overall the waveforms from simulation match well with those from experiment, at least for the low order components.

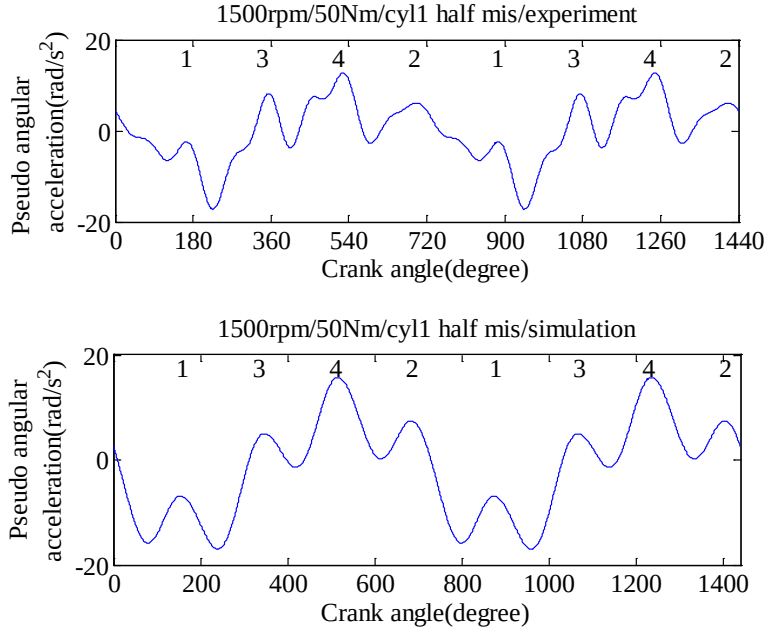

Figure 28. Experimental and simulated pseudo angular accelerations of the engine block for the 50% misfires in cylinder 1

The polar diagrams for the simulated pseudo angular accelerations of the block were investigated as well. Two examples at 1500rpm/50Nm and 3000rpm/50Nm are shown in Figure 29. Again, as mentioned in preceding section, the most useful information for the misfire diagnosis from the pseudo angular accelerations of the block is the amplitude ratio of the 1st harmonic to the 4th harmonic and the phase of the 1st harmonic. From Figure 29, it can be found that even though the remaining harmonic information is not accurate, the simulated amplitude ratio of the 1st harmonic to the 4th harmonic matches with the experimental results. Additionally, because the combustion force frequencies change at different engine speeds, but the FRFs of the rigid body motions of the engine block remain fixed, the phase of the 1st

harmonic is only fixed at a certain speed. It can be seen that at different speeds, the phase changes of the 1st harmonic were correctly simulated.

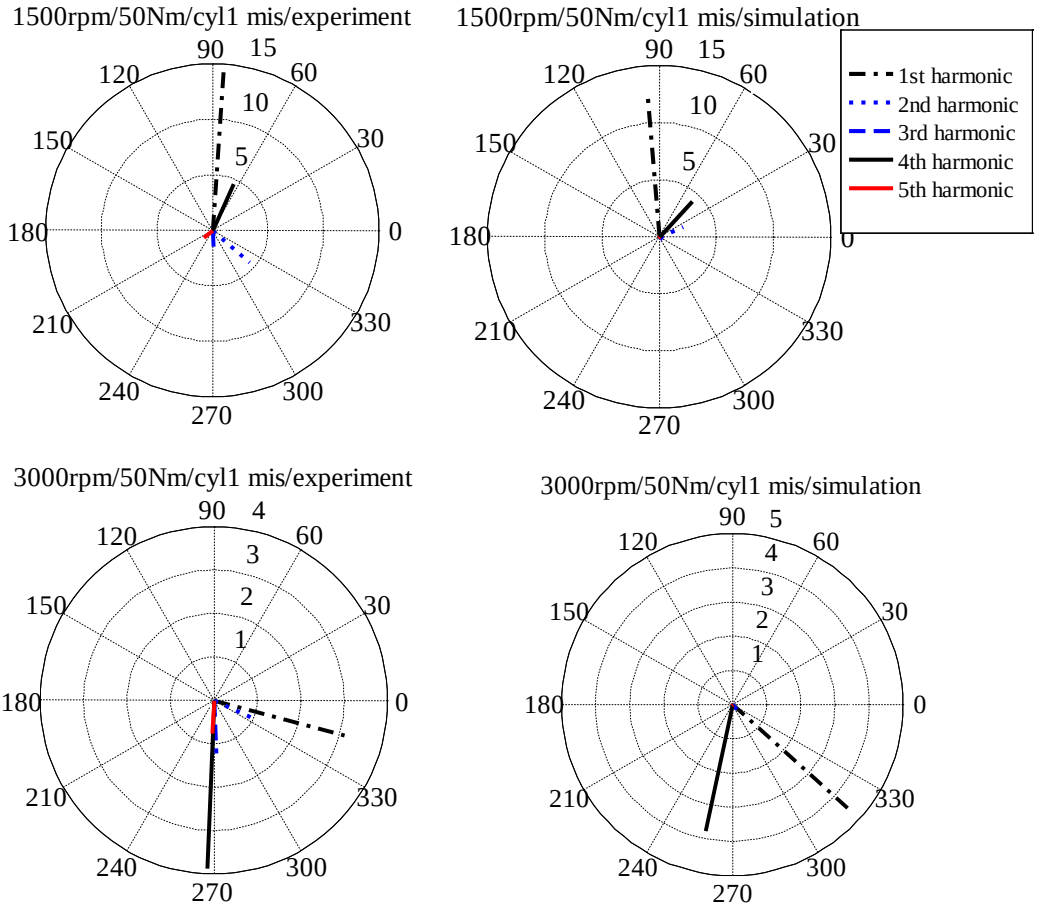

Figure 29. Polar diagram of the experimental and simulated pseudo angular accelerations of engine block for the misfires in the cylinder 1

Compared to the errors from the simulation of torsional vibration, the errors of the simulated pseudo angular accelerations of engine block are bigger. That is because it is not easy to obtain accurate inertia properties for the engine and the properties of the engine mounts. The experimental pseudo angular accelerations of the block were measured under operational conditions, but the inertia properties of the engine and properties of the engine mounts were measured in static conditions. The noise contamination is also difficult to simulate in the models. Because both simulation models are 1D, the computing time is not very long. For 3 seconds of engine running simulated period (75 revaluations for 1500rpm), the computing time for torsional vibration model is about 5 minutes, and for pseudo angular accelerations of engine block is about 10 minutes, including the calculation from the simulated genuine angular accelerations to the simulated pseudo angular accelerations.

4. Automated diagnosis of misfires

It is worth pointing out that the engine outputs (load and speed) are precisely controlled by the dynamometer, but the combustion in the experiments was still affected by some uncontrollable ambient environment factors, such as temperature. The experimental period ranged over 6 months in year 2010 (July to December), and the ambient temperature had over 20 degrees variation, therefore it was found that there are some variations in the processed experimental signals (up to 5% variation in the same normal condition but different experiment times), for both torsional vibration and engine block angular acceleration. However, the ANN trained by a large amount of training data can overcome the variation of the input vector and accurately classify different combustion faults. On the other hand, the simulated signal for a certain speed/load condition is deterministic, so a variation in the simulated signals should be introduced to create representative cases for the ANN training. The standard deviation of the variations was set by analysing the

normal conditions from experiments and was applied to all the simulated signals, including normal conditions and faulty conditions.

A three-stage system was designed for the automated misfire diagnostics (as shown in Figure 30). Misfire can be detected in the first stage. In the second stage, the cylinder which has a misfire can be identified. In the third stage, based on the detection results, the severity of the misfires can be identified. The most important thing for the fault diagnostics is to find the features to represent different misfires. As studied in the preceding section, for both torsional vibration and pseudo angular accelerations, it was found that the amplitude ratios of the 1st harmonic to the 4th harmonic (for a four cylinder, four stroke engine) can be used to detect the misfires and identify the severity. Moreover, the phase of the 1st harmonic can be used to classify which cylinder has the misfire. Therefore, the amplitude ratios of the 1st harmonic to the 4th harmonic were the input vectors to the detection stage and severity identification stage and the phases of the 1st harmonic were the input vectors to the localization stage.

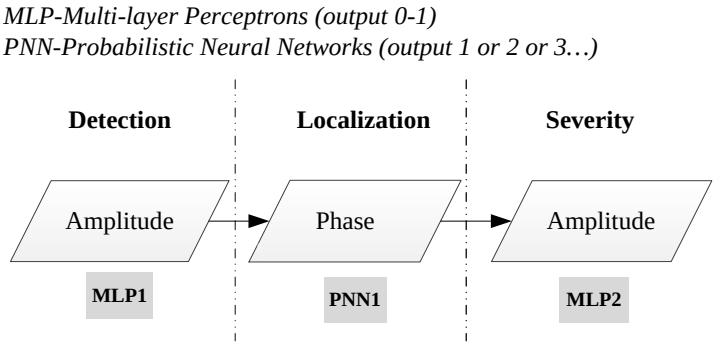

Figure 30. Structure of the three-stage ANN system

Feed-forward MLP neural networks were used to detect whether there are misfires and to identify the severity of misfire. Two MLPs were designed: one for the fault detection (MLP1) and the other for the severity identification (MLP2). The MLPs consist of three layers: input, hidden and output. The numbers of hidden neurons of the MLPs were determined using a trial and error procedure. There are two transfer functions corresponding to each layer and the output of the MLPs is from 0 to 1. In our former works [33-35], we used a nonlinear log sigmoid transfer function in the hidden layers for both MLP1 and MLP2. Definitely, for the detection stage (MLP1), the log sigmoid function was the best function to use, and it enabled all cases to converge to two boundary conditions 0 and 1, 0 for normal condition and 1 for misfire. In the severity stage (MLP2), however, the log sigmoid function also attempts to nonlinearly classify all cases at specified levels of misfire, but this does not agree with the real situation (the severity level of misfires should be any value linearly distributed from 0 to 1). Even though we were able to use a lot of training data to train the MLP2 to get a correct classification of the three levels of misfire (as shown in the former papers), the results were not the best and the classification is coarse. Therefore, in the new design of MLP2, saturating linear transfer functions satlin(x) were introduced into both layers. The diagram of an MLP2 is shown in Figure 31. This satlin(x) function is linear in the interval (-1,+1) and saturates outside this interval to -1 or +1. It returns the value of x truncated into the range 0 to 1. I_w and b are respectively the weight and bias factors distributed to the individual elements of the input feature vectors. During the training stage, the MLPs were led to a specific target output by adjusting the values of the connections (weights and bias) among the elements of the input vectors. The number 30 means the number of neurons in the hidden layer. The output of MLP2 can be any value linearly distributed from 0 to 1, for instance, 0.2 represents 20% misfire, 0.5 for 50% misfire and 1 for 100% misfire. Meanwhile, in the former works, we tried to use one MLP to identify the severity levels for all speed and load conditions, but actually the variation of the input vectors for different speeds and loads is large, and gave another reason for the coarse classification of the severity level. In order to get finer classification, after analysing the experimental and simulation data, it was found that the variation of amplitude ratios is more sensitive to the speeds than the loads, so three separate MLPs were designed for three different speed conditions (1500rpm, 2000rpm and 3000rpm) in the new MLP2. Note that the idea of “one MLP2 for one speed” is also feasible in the real industrial situation, because it is always easy to measure and know the speed of the engine during the condition monitoring process.

The MLPs were trained for up to 500 epochs to an error goal of 0.001. The training status is displayed for every 5 epochs. The learning rate is set as 0.001 and the momentum constant was set as 1.

```
net.trainParam.show = 5;
net.trainParam.lr = 0.001;
net.trainParam.mc = 1;
net.trainParam.epochs = 500;
net.trainParam.goal = 0.001;
```

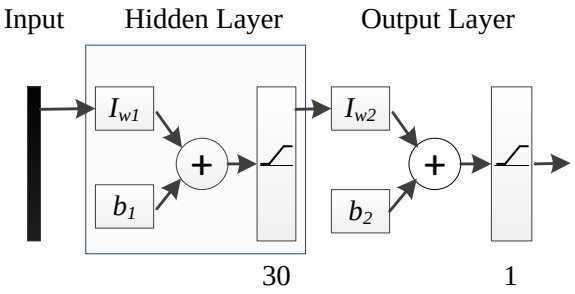

Figure 31. The diagram of the MLP2 with saturating linear transfer functions

Due to its advantage for classification problems, a PNN was used to identify which cylinder has misfires. The PNN is based on the weighted-neighbour method and was proposed by Specht [54]. The distance is computed from the point being evaluated to each of the other points, and a radial basis function is applied to the distance to compute the weight for each point. The training of the PNN is a simple implementation of a Parzen nonparametric probability density function estimator and Bayesian decision rule. For each new training sample x belonging to c_i class, the training process adds a new neuron in the i th pool of the pattern layer, with the weight vector which is x; this non-iterative training procedure is very fast. The structure of a typical PNN is shown in Figure 32. The outputs of the PNN for the misfire diagnostics are the integer numbers 1, 2, 3 and 4, which directly indicate the cylinder number.

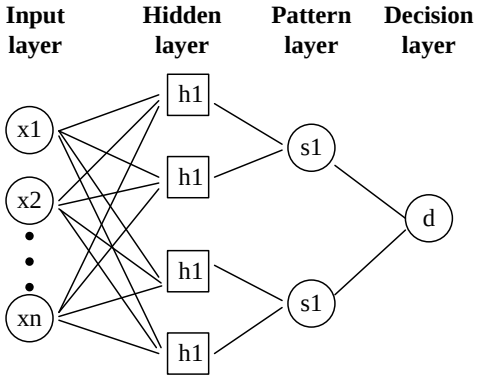

Figure 32. The diagram of the PNN networks.

Only the simulated data was used to train the networks and the experimental cases were used to test the performance of the networks. The simulated signal for a certain speed/load condition is deterministic, but in reality the measurement signals have small deviations in different test scenarios, so as mentioned above a variation in the simulated signals should be instituted to create representative cases for the ANN training. The standard deviation of the variations was set by analysing the normal conditions from experiments and was applied to the simulated signals. Normal conditions at each speed and load were simulated and twenty variations were created for each simulated normal condition. Both 50% and 100% misfires were also simulated in different cylinders for each speed and load condition and all the simulated signals were instituted with variations (five variations for each simulation).

Table 1: Distribution of data with networks from simulation and experiment

for training (simulation)			for test (experiment)		
normal	100% misfire	50% misfire	normal	100% misfire	50% misfire
180 in total	180 in total, *45 in cylinder 1* *45 in cylinder 2* *45 in cylinder 3* *45 in cylinder 4*	180 in total, *45 in cylinder 1* *45 in cylinder 2* *45 in cylinder 3* *45 in cylinder 4*	15 in total	19 in total, *9 in cylinder 1* *7 in cylinder 2* *3 in cylinder 3*	2 in total, *2 in cylinder 1*

540 cases from the simulation were used to train the system, including 180 normal conditions and 360 misfire conditions. 36 cases from the experiments were used to test the system, including 15 normal conditions and 21 misfire conditions. The distribution of the different conditions is shown in Table 1. In the MLP1, the 540 amplitude ratios were input into the network. After the detection stage, the training and test cases for the PNN were reduced to the group of all cases with misfires (misfires in different cylinders). Likewise, the training and test cases for the MLP2 were reduced too, so the severity identification became more specific. It is noteworthy that the purpose of the paper is to simulate sufficient data for the training, so the number of training cases is not a big problem to get optimum performance of the ANNs and the minimum number of training cases required to achieve 100% ANN results was not investigated in this paper.

A fitness criterion was introduced to evaluate the performance of the MLP1:

$$Error = \sum_{i=1}^{N} \left| (ANN(i) - VAL(i) \right| / N \tag{5}$$

where *ANN* is the output of the MLP1 and *VAL* is the corresponding target number. *N* is the total number of the test group (33). A higher fitness criterion means poorer MLP performance. Because the log sigmoid transfer function is very good at the problem of classification of two groups, and our former works [33-35] also demonstrated that the speeds and loads are not necessary inputs for the classification of MLP1, only one MLP1 was designed to detect the misfire at all speed and load conditions and the input of MLP1 is a 1D vector (amplitude ratio of the 1st harmonic to the 4th harmonic). Due to the simple dimension of the input vector and the clear difference between the input features of normal conditions and those of misfire conditions, the computing time for the MLP1 is short, from 0.6-1 seconds. The results of MLP1 are shown in Table 2. It can be seen that results are good, with 100% correct and very small error values. Meanwhile, it can be seen that because the pseudo angular acceleration is subject to more complicated influences and is more difficult to simulate, its fitness criteria are worse than those for the torsional vibration method.

It is worth pointing out that as mentioned in the preceding section, for the torsional vibration the phases of the 1st harmonic with misfire in a certain cylinder are nearly fixed for any speed/load condition, so the inputs to the PNN for torsional vibration have only one element (the phases of the 1st harmonic), but for the pseudo angular acceleration methods, the phases of the 1st harmonic with misfire are only fixed at a certain speed, so the inputs to the PNN for the pseudo angular acceleration method definitely have to include the phases of the 1st harmonic and the speed. The computing time for the PNN of the torsional vibration method is 0.3-0.5 seconds, and for the PNN of pseudo angular acceleration method, a little longer, from 0.5-0.8 seconds. As mentioned before, the outputs of the PNN are the integer numbers 1, 2, 3 and 4, which directly indicate the cylinder number. The final results have also shown that the PNN successfully localized which cylinder has misfire: eleven cases in cylinder 1, seven cases in cylinder 2 and three cases in cylinder 3.

Table 2: Comparison for the results of the MLP1

	Detection(MLP1)
Torsional vibration of crankshaft	100% correct error=0.4941
Angular acceleration of engine block	100% correct error=0.5819

Table 3: Comparison for the results of two MLP2 designs

	Old MLP2 Design		New MLP2 Design	
	100% misfire	50% misfire	100% misfire	50% misfire
Torsional vibration	output range 0.972-1	output range 0.548, 0.483	output range 0.991-1	output range 0.512, 0.495
Angular acceleration	output range 0.947-0.992	output range 0.621, 0.446	output range 0.984-1	output range 0.523, 0.488

Three MLPs with saturating linear transfer functions were designed for the severity identification of each speed condition. Likewise, the amplitude ratio of the 1st harmonic to the 4th harmonic is the only input to the three MLPs. As mentioned before, the old MLP2 (only one MLP) with log sigmoid transfer function was used to identify the severity level at all speed and load conditions. Therefore, in order to compare the results and show the improvement of the newly designed MLP2, the number of the total training cases (360) and the number of the total test cases (21) are same for both old and new MLP designs and the results of the three MLPs are combined together and shown in Table 3. It can be seen that, even though both the old MLP2 and new MLP2 can identify the levels of the misfire faults, the new MLP2 has a much finer classification, especially for the two experimental cases with 50% misfire. If there were an experimental case with 60% misfire, the old MLP2 would mix it with the 50% misfire case, but the new MLP2 could efficiently classify the problem. The computing times for both old and new MLP2 are very similar, from 0.5-1 second.

5. Conclusion

ANN-based automated systems were developed for the diagnosis of misfire. In order to obtain sufficient results for the network training, simulation models, which can simulate different locations and ranges of misfires, were developed in this paper. The simulation models need to be evaluated and updated using the experimental data, so experimental vibration signals with combustion faults were studied first. It was found that the torsional vibration of the crankshaft and the pseudo angular acceleration of the engine block can both be used to diagnose engine misfires. Meanwhile, as inputs to the simulation models, the inertial properties of the engine components and the parameters of the engine mounts were also measured and/or calculated. The simulation models are based on the thermodynamic and mechanical principles of IC engines and therefore the proposed diagnostic system can in principle be adapted for any engine. The automated system was trained purely by simulation data and tested using the experimental data, showing that it is possible to generate a simulation model which gives confidence in its application to a somewhat wider range of fault locations and severities, provided these remain within the overall envelope of the physical conditions for which the model has been validated. The diagnosis consists of three stages: MLP1 for the detection stage, PNN for the localization stage and MLP2 for the severity identification stage. For both the torsional vibration method and the pseudo angular acceleration method, the amplitude ratios of the 1st harmonic to the 4th harmonic were used for the misfire detection and severity identification, and the phase of the 1st harmonic was used for the misfire localization. In particular, for the severity identification stage, separate MLPs with saturating linear transfer functions were designed for the three speed conditions, so the outputs of the MLP2 can be any value linearly distributed from 0 to 1. Finally, it was demonstrated that the networks trained on simulated data can efficiently detect misfire in real tests and identify the location. More importantly, compared to results from the old MLP2, the new MLP2 can obtain a much finer classification of the severity of the misfires.

Acknowledgements

The authors would like to convey special gratitude to the Australian Research Council and LMS International for sponsoring this research under Linkage Project LP0883486. Special thanks to Professor

Asoke Nandi of Brunel University London, for his helpful discussions and suggestions on the design of MLPs during the Surveillance 7 conference in Chartres, France.

References

[1] R. G. DeJong, R. E. Powell, J. E. Manning, Engine monitoring using vibration signals, SAE No. 861246, 1986.

[2] R. H. Lyon, L. T. Kim, Recovery of fault signatures in diesel engines, SAE No. 880824, 1988.

[3] J. T. Kim, R. H. Lyon, Cepstral analysis as a tool for robust processing, deverberation and detection of transients, Mechanical Systems and Signal Processing 6 (1) (1992)1-15.

[4] Y. Gao, R. B. Randall, Reconstruction of diesel engine cylinder pressure using a time domain smoothing technique, Mechanical Systems and Signal Processing 13 (5) (1999) 709-722.

[5] P. Azzoni, M. Marseguerra, Assessment of the potential of a Wiener-Hilbert filter for automatic diagnosis of spark ignition engine faults, Mechanical Systems and Signal Processing 9 (2) (1995) 119-128.

[6] J. Chang, M. Kim, K. Min, Detection of misfire and knock in spark ignition engines by wavelet transform of engine block vibration signals, Measurement Science and Technology 13 (7) (2002)1108-1114.

[7] J. Antoni, J. Daniere, F. Guillet, R. B. Randall, Effective vibration analysis of IC engines using cyclostationarity. Part II – New results on the reconstruction of the cylinder pressures, Journal of sound and vibration 257 (6) (2002) 839-856.

[8] S. J. Citron, J. E. O'Higgins, L. Chen, Cylinder by cylinder engine pressure and pressure torque waveform determination utilizing speed fluctuations, SAE No. 890486, 1989.

[9] H. Fehrenbach, Model-based combustion pressure computation through crankshaft angular acceleration analysis. 22nd International Symposium on Automotive Technology and Automation, Florence, Italy, (1990) 639–647.

[10] T. S. Brown, W. S. Neill, Determination of engine cylinder pressures from crankshaft speed fluctuations, SAE No 920463, 1992.

[11] J. Williams, An overview of misfiring cylinder engine diagnostic techniques based on crankshaft angular velocity measurements, SAE Paper 960039, 1996.

[12] U. Kiencke, Engine misfire detection, Control Engineering Practice 7 (1999) 203-208.

[13] J. Yang, L. Pu, Z. Wang, Y. Zhou, X. Yan, Fault detection in a diesel engine by analysing the instantaneous angular speed, Mechanical Systems and Signal Processing 15 (3) (2001) 549–564.

[14] J. J. Moskwa, W. Wang, D. J. Bucheger, A new methodology for engine diagnostics and control utilizing 'synthetic' engine variables: theoretical and experimental results, Transactions of the ASME: Journal of Dynamic Systems, Measurement, and Control 123 (2001) 528-534.

[15] A. W. Osburn, T. M. Kostek, M. A. Franchek, Residual generation and statistical pattern recognition for engine misfire diagnostics, Mechanical Systems and Signal Processing 20 (8) (2006) 2232-2258.

[16] Y. Zhang, R. B., Randall, The In-Cylinder Pressure Reconstruction and Indicated Torque Estimation Based on Instantaneous Engine Speed and one Measured In-Cylinder Pressure, Comadem Conference, Faro, Portugal, 12–15 June 2007.

[17] P. Charles, J. K. Sinha, F. Gu, L. Lidstone, A. D. Ball, Detecting the crankshaft torsional vibration of diesel engines for combustion related diagnosis, Journal of Sound and Vibration 321 (3–5) (2009) 1171–1185.

[18] P. Charles, J. K. Sinha, F. Gu, A. D. Ball, Application of novel polar representation method for monitoring minor engine condition variations, Mechanical Systems and Signal Processing 24 (3) (2010) 841–843.

[19] M. Desbazeille, R. B. Randall, F. Guillet , M. El Badaoui, C. Hoisnard, Model-based diagnosis of large diesel engines based on angular speed variations of the crankshaft, Mechanical Systems and Signal Processing 24 (5) (2010) 1529–1541.

[20] J. K. Ball, M. J. Bowe, C. R. Stone, P. D. McFadden, Torque estimation and misfire detection using block angular acceleration, SAE Technical Paper No. 2000-01-0560, 2000.

[21] V. Macián, M. Lerma, D. Barilá, Condition monitoring of thermal reciprocating engines through analysis of rolling block oscillations, SAE Technical Paper No. 980116, 1998.

[22] V. Macian, A. Broatch, B. Tormos, P. Olmeda, Methodology of fault detection in internal combustion engines through the analysis of rolling block oscillation, International Journal of Heavy Vehicle Systems 16 (3) (2009) 294-309.

[23] W. J. Hardman, C. G. Neubert, Detection of bearing faults in operational SH-60B aircraft main transmission module by vibration analysis, controls and diagnostics division, Air-4.4.2, United States Navy, Naval Airwar Center, Aircraft Division, TRENTON-LR-PPE-96-7, USA, 1996.
[24] G. M. Knapp and H. P. Wang, Machine fault classification: a neural network approach, International Journal of Production Research 30 (4) (1992) 811-823.
[25] B. Li, M. Y. Chow, Y. Tipsuwan, J. C. Hung, Neural-network-based motor rolling bearing fault diagnosis, IEEE Transactions on Industrial Electronics 47 (5) (2000) 1060-1069.
[26] A. J. Hoffman, N. T. Van der Merwe, The application of neural networks to vibrational diagnostics for multiple fault conditions, Computer Standards & Interfaces 24 (2) (2002) 139-149.
[27] B. Samanta, K. R. Al-Balushi, Artificial neural network based fault diagnostics of rolling element bearings using time domain features, Mechanical Systems and Signal Processing 17 (2) (2003) 317-328.
[28] V. Crupi, E. Guglielmino, G. Milazzo, Neural-network-based system for novel fault detection in rotating machinery, Journal of Vibration and Control 10 (8) (2004) 1137-1150.
[29] H. Nahvi, M. Esfahanian, Fault identification in rotating machinery using artificial neural networks, Proceedings of the Institution of Mechanical Engineers, Part C: Journal of Mechanical Engineering Science 219 (2) (2005) 141-158.
[30] J. Rafiee, F. Arvani, A. Harifi, M. H. Sadeghi, Intelligent condition monitoring of a gearbox using artificial neural network, Mechanical Systems and Signal Processing 21 (4) (2007) 1746-1754.
[31] L. B. Jack, A. K. Nandi, Fault detection using support vector machines and artificial neural network, augmented by genetic algorithms, Mechanical System and Signal Processing 16 (2-3) (2002) 373–390.
[32] R. B. Randall, The application of fault simulation to machine diagnostics and prognostics, Keynote lecture, Proceedings of the 16th International Congress on Sound and Vibration, Krakow, Poland, 5-9 July 2009.
[33] J. Chen, R. B. Randall, B. Peeters, H. Van der Auweraer, W. Desmet, Automated misfire diagnosis in engines using torsional vibration and block rotation, COMADEM2012, Huddersfield, UK, 18-20 June 2012.
[34] J. Chen, R. B. Randall, Use of block pseudo angular acceleration for engine misfire diagnosis, Acoustics 2013, Victor Harbor, Australia, 17-20 November 2013
[35] J. Chen, R. B. Randall, N. Feng, B. Peeters, H. Van der Auweraer, Automated diagnostics of internal combustion engine using vibration simulation, Surveillance 7, Chartres, France, 29-30 October 2013.
[36] K. Janssens, L. Britte, Comparison of torsional vibration measurement techniques, International Conference on Noise and Vibration Engineering, Leuven, Belgium, 17-19 September, 2012.
[37] P. D. McFadden, Detecting fatigue cracks in gears by amplitude and phase demodulation of the meshing vibration, Transactions of the ASME - Journal of Vibration, Acoustics, Stress, and Reliability in Design 108 (1986) 165–170.
[38] P. J. Sweeney, R. B. Randall, Gear transmission error measurement using phase demodulation. Proceedings of the Institution of Mechanical Engineers, Part C: Journal of Mechanical Engineering Science 210 (C3) (1996) 201–213.
[39] A. Y. B. Sasi, F. Gu, B. Payne, A. D. Ball, Instantaneous angular speed monitoring of electric motors, Journal of Quality in Maintenance Engineering 10 (2) (2004) 123-135.
[40] J. Bretl, P. Conti, Rigid body mass properties from test data, Proceeding of the 5th Intentional Modal Analysis Conference, London, England, (1987) 655-659.
[41] N. Okubo, T. Furukawa, Measurement of rigid body modes for dynamic design, Proceedings of the 2nd Intentional Modal Analysis Conference, Florida, USA (1984) 545-549.
[42] A. Fregolent, A. Sestieri, Identification of rigid body inertia properties from experimental data, Mechanical Systems and Signal Processing 10 (6) (1996) 697–709.
[43] M. C. Witter, D. L. Brown, J. R. Blough, Measuring the six DOF driving point impedance function and an application to RB inertia property estimation, Mechanical Systems and Signal Processing 14 (1) (2000) 111-124.
[44] E. Mucchi, G. Bottoni, R. Di Gregorio, Indirect measurement of the inertia properties of a knee prosthesis through a simple frequency-domain technique, Transactions of the ASME: Journal of Medical Devices, 3 (4) (2009) 044501.1-045001.7.
[45] R. A. B. Almeida, A. P. V. Urgueira, N. M. M. Maia, Further developments on the estimation of rigid body properties from experimental data, Mechanical Systems and Signal Processing 24 (5) (1999) 1391–1408.

[46] P. Conti, J. Bretl, Mount stiffness and inertia properties from modal test data, Transactions of the ASME: Journal of Vibration, Acoustic, Stress and Reliability in Design 111 (1989) 134– 138.
[47] S. M. Pandit, Z. Q. Hu, Determination of rigid body characteristics from time domain modal test data, Journal of Sound and Vibration 177 (1) (1994) 31-41.
[48] J. Chen, R. B. Randall, B. Peeters, H. Van der Auweraer, W. Desmet, Inertial property estimation by the modal model method, International Conference on Noise and Vibration Engineering, Leuven, Belgium, 17-19 September, 2012.
[49] C. F. Taylor, The internal combustion engine in theory and practice, Volume 2: combustion fuel material and design, MIT press, Cambridge Massachusetts, USA, 1968.
[50] J. I. Ghojel, Review of the development and applications of the Wiebe function: a tribute to the contribution of Ivan Wiebe to engine research, International Journal of Engine Research 11 (4) (2010) 297-312
[51] J. Chen, R. B. Randall, A vibration signal based simulation model for the misfire of internal combustion engines, CM & MFPT2011, Cardiff, UK, June 20-22 2011.
[52] J. P. Den Hartog, Mechanical vibrations, Dover Publications, New York, USA, 1985.
[53] W. Ker Wilson, Practical solution of torsional vibration problems, John Wiley & Sons Inc. New York, USA, 1963.
[54] F. D. Specht, Probabilistic neural networks and the polynomial adaline as complementary techniques for classification, IEEE Transactions on Neural Networks 1 (1) (1990) 111-121.